

ANALYSIS OF ANTARCTIC SEA ICE THICKNESS: A NEWLY CREATED
DATABASE FOR 2000-2009

A Thesis

by

BENJAMIN PATRICK MORGAN

Submitted to the Office of Graduate Studies of
Texas A&M University
in partial fulfillment of the requirements for the degree of

MASTER OF SCIENCE

August 2011

Major Subject: Oceanography

Analysis of Antarctic Sea Ice Thickness: A Newly Created Database for 2000-2009

Copyright 2011 Benjamin Patrick Morgan

ANALYSIS OF ANTARCTIC SEA ICE THICKNESS: A NEWLY CREATED
DATABASE FOR 2000-2009

A Thesis

by

BENJAMIN PATRICK MORGAN

Submitted to the Office of Graduate Studies of
Texas A&M University
in partial fulfillment of the requirements for the degree of

MASTER OF SCIENCE

Approved by:

Co-Chairs of Committee,	Alejandro H. Orsi
	Achim Stoessel
Committee Member,	Andrew G. Klein
Head of Department,	Piers Chapman

August 2011

Major Subject: Oceanography

ABSTRACT

Analysis of Antarctic Sea Ice Thickness: A Newly Created Database for 2000-2009.

(August 2011)

Benjamin Patrick Morgan, B.S., United States Coast Guard Academy

Co-Chairs of Advisory Committee: Dr. Alejandro H. Orsi
Dr. Achim Stoessel

Observations of Antarctic sea ice thickness are sporadic in space and time, hindering knowledge of its variability. A proxy based on stage of development data from the National Ice Center (NIC) weekly operational charts is used to create a high-resolution time series of sea ice concentration, thickness and volume for 2000-2009.

Record-length mean thickness and volume of Antarctic sea ice are 66.7 cm and 7.7×10^3 km³. The mean growth and decay seasons in the Southern Ocean and in the Ross sector are 210 days and 155 days, but at least at least one week shorter (growth) and longer (decay) in the Amundsen/Bellingshausen sector. Over 90% of the Antarctic continental shelf is covered with sea ice for 3-5 months, and for 2 to 4 months longer periods in the Amundsen/Bellingshausen and Ross sectors.

Yearly mean sea ice area (extent) in the Southern Ocean increased at a rate of 0.71×10^6 km²/decade (0.70×10^6 km²/decade), equivalent to a 7.7 %/decade (6.3 %/decade) rise. A comparable trend of 9.1 %/decade (8.5 %/decade) is estimated in the Ross sector, at 0.21×10^6 km²/decade (0.23×10^6 km²/decade). The opposite trend is found in the Amundsen/Bellingshausen sector: a -0.15×10^6 km²/decade (-0.17×10^6 km²/decade) decline, or -14.6 %/decade (-13.4 %/decade).

The estimated annual increase of Antarctic sea ice thickness is 22.6 cm/decade (49.2 %/decade) and of volume is $3.78 \times 10^3 \text{ km}^3/\text{decade}$ (68.3 %/decade). The Ross sector showed similar trends for thickness, at 23.8 cm/decade (47.0 %/decade), and volume, at $1.11 \times 10^3 \text{ km}^3/\text{decade}$ (75.8 %/decade). Thickness has increased in the Amundsen/Bellingshausen sector, 20.7 cm/decade (44.8 %/decade), but with a less pronounced volume rise of $0.17 \times 10^3 \text{ km}^3/\text{decade}$ (26.0 %/decade).

Monthly sea ice thickness anomalies show a weak response to the El Niño Southern Oscillation (ENSO) index. A strong positive response is observed in 2008 when a negative ENSO index compounded to a positive Southern Annular Mode (SAM) index. Therefore the estimated increase of sea ice thickness in the Southern Ocean could be attributed to the prevailing atmospheric conditions with a positive SAM phase over the past decade.

DEDICATION

This work is dedicated to my late grandfathers, Warren E. Morgan and Jeremiah L. Maher. With tireless work ethic and impeccable integrity, both bore great burdens and responsibilities during some of our nation's greatest trials without a college education or so much as a complaint. The former taught me the importance of continuous learning, because: "education is something no one can ever take away from you." The latter taught me to pursue big dreams and encouraged my exploration to the ends of the earth. Both of these role models will forever be larger than life to me and were instrumental in shaping me into the man (husband, father, citizen, officer and student) I am today... or at least the benchmark to which I will always aspire.

ACKNOWLEDGEMENTS

I have never been one to shy away from “the road less traveled,” although it can, on occasion, be debated whether I directly chose that road or whether it chose me. Regardless of the case, there have always been those who stood by me and helped me overcome each challenge. This project is no exception and would not have been possible without the support of the following people and organizations:

First and foremost, I must thank the United States Coast Guard, and indirectly the American taxpayer, for subsidizing my advanced education. It has been an honor and a privilege to serve in this capacity as an officer and oceanographer. I am eternally grateful for the opportunities and experiences I have been afforded in the service. I would also like to extend my heart-felt gratitude to the Webbers for their financial support through the Webber Fellowship.

I am very grateful to be able to work with some of the greatest researchers in Antarctic geosciences. I thank my committee members Dr. Alejandro Orsi, Dr. Achim Stoessel and Dr. Andrew Klein for their support of, and interest in, my research and education. All three were directly involved in this project, allowed me to chose my own path (or dig my own hole) and provide appropriate correction, direction and guidance along the way. I also wish to thank Dr. Orsi for providing me the opportunity to gain insight and experience in the world of operational oceanography. It was most certainly an adventure I will never forget.

I wish to thank the faculty, staff and students at Texas A&M University and, more specifically, those in the Department of Oceanography for welcoming me into their community and making my graduate school experience enjoyable and complete. In particular, I thank my officemates in the small, but elite, Southern Ocean Research Group (SORG)- Chrissy Wiederwohl, YongSun Kim and, by proxy, Kelly Cole. In

addition to providing ample respites from the daily grind of graduate student life, these fellow graduate students were incredibly patient and helpful as they constructively critiqued my work, provided generous encouragement and taught me the complex tools and techniques of our unique field of study. Chrissy, above all, devoted a large amount of her own time to helping me. There were times when her encouragement and positive attitude were the only things that kept my faith in this project. I am tremendously grateful for her help and am certain I could not have succeeded otherwise.

Most recently, I have received tremendous support and encouragement from my current command at U.S. Coast Guard Headquarters. Specifically, I wish to thank LCDR Michael Krause and Mr. Douglas Jackson for their interest in helping me succeed. Their extra efforts and kindness did not go unnoticed.

The foundations for my advanced education were laid long before I ever arrived at Texas A&M University. The instructors at my Alma Mater, the United States Coast Guard Academy, did a phenomenal job, not only preparing me for a career as an officer, but also sparking my interest in marine science and preparing me for graduate school. No one is more responsible for my interest in the cryosphere and the polar sciences than the late Dr. Douglas “Doc T” Tolderlund. I was indeed fortunate to be among the last classes of the Corps of Cadets to benefit from his passion, experience and knowledge before his retirement in 1999. It was his lecture on glaciers and polar ice in the marine geology course that made me decide to become a polar icebreaker sailor. I am also deeply appreciative of the support and inspiration provided by my officer/oceanographer mentors CAPT Steven Nerheim, USN (ret.); CAPT Michael Alfultis, USCG (ret.); and CDR Scott Rogerson, USCG (ret.). I believe these three gentlemen are among our nation’s finest leaders and scientists.

My entire family has always been an invaluable source of support and encouragement through all of my life pursuits. Not only were my parents shining examples of

dedication, perseverance and self-discipline (as their parents before them), but they also love me unconditionally. I can never thank them enough, for I know they made great sacrifices in order to provide me countless opportunities. I carry their guidance with me always. Of course, I would also be remiss if I did not also acknowledge the contributions of my two brothers, Andrew and Nicholas, who provided motivation by being quick to point out that I am “the least educated” of the Morgan boys... that is, until now. I thank them for providing the not-so-gentle nudge I occasionally need. I also thank Mike and Sue, my other parents, for their support of my career and family, even though it meant moving their firstborn child (and only daughter) so far away from home.

Most of all, I owe the deepest debt of gratitude to my beautiful wife, Sara. I have heard it said, through various disparate sources, that there is no harder job than being a military spouse, a mother, a mother of multiples, the wife a graduate student or being the wife of Ben Morgan. My wife has simultaneously held all of these positions and, I am very proud to say, has done so with remarkable grace and poise. Sara is the wind in my sails and the inspiration for all that I do. I know that there were many late and lonely nights, and that many times she bore the burden of my absence. Sara is always willing to go where I go in pursuit of elusive dreams and demonstrates incredible strength while holding our home together. I am humbled by her faith and devotion.

Finally, I am immensely blessed and inspired by my two sons, who were born during this research. I am certain “Every good and perfect gift is from above...” (James 1:17). May they grow to be stronger and smarter than their father....

NOMENCLATURE

AABW	Antarctic Bottom Water
ACC	Antarctic Circumpolar Current
AIDJEX	Arctic Ice Dynamics Joint Experiment
ASPeCt	Antarctic Sea Ice Processes and Climate
DMSP	Defense Meteorological Satellite Program
ENSO	El Nino-Southern Oscillation
MOC	Meridional Overturning Circulation
NIC	National Ice Center
NOAA	National Oceanographic and Atmospheric Administration
SAM	Southern Annular Mode
SIGRID	Sea Ice Gridded
SIRAL	Synthetic Aperture Radar (SAR)/Interferometric Radar Altimeter
SMMR	Scanning Multichannel Microwave Radiometer
SSMI	Special Sensor Microwave/Imager
SW	Shelf Water
ULS	Upward-Looking Sonar
WAP	Western Antarctic Peninsula
WMO	World Meteorological Organization

TABLE OF CONTENTS

	Page
ABSTRACT	iii
DEDICATION	v
ACKNOWLEDGEMENTS	vi
NOMENCLATURE	ix
TABLE OF CONTENTS	x
LIST OF FIGURES	xii
LIST OF TABLES	xv
1. INTRODUCTION.....	1
1.1 Background	7
1.2 Objectives.....	12
2. DATA AND METHODS.....	13
2.1 ASPeCt Data	13
2.2 NIC Data	14
2.3 Quality Control of NIC Data.....	16
2.4 Source Data Errors	18
2.5 Gridded NIC Data	19
3. DATA COMPARISON.....	20
4. ANALYSIS AND RESULTS	25
4.1 Sea Ice Extent and Area: Decadal and Inter-annual Variability	26
4.2 Duration of Sea Ice Seasons.....	35
4.3 Surface Coverage	37
4.4 Sea Ice Thickness	37
4.5 Sea Ice Volume	44
4.6 Relationship to Atmospheric Inter-annual Variability	48

	Page
5. DISCUSSION AND CONCLUSIONS.....	54
REFERENCES.....	57
VITA	60

LIST OF FIGURES

FIGURE	Page
1	Flow chart depicting the stages of sea ice development, which depends on oceanographic conditions 3
2	Model ridge and the components where R is the fractional coverage of ridges, S is the average sail height of ridges, Z_u is the average level ice thickness and Z_r is the mean thickness 3
3	Sample of the World Meteorological Organization (WMO) "egg code" ice reporting protocol 6
4	Example of a sample egg code converted to a SIGRID 7
5	Schematic of positive phase SAM influence on atmospheric and oceanic circulation 8
6	Schematic of a positive SAM phase and impact on sea ice from <i>Stammerjohn et al.</i> [2008] 9
7	Sea surface temperature anomalies and atmospheric variability associated with the positive phase of the El Niño Southern Oscillation, and the negative phase 11
8	Geographic representation of all ASPeCt observations 14
9	Example of NIC weekly ice chart polygons from November 2000 15
10	Example weekly ice chart displaying calculated ice thickness values for 04-10 January 2000 18
11	Comparison of ice chart polygon thickness and mean ASPeCt observed thickness in the Amundsen/Bellingshausen sector demonstrating a relatively high goodness of fit with relatively few data points 22
12	Comparison of southern hemisphere ice thickness using the nearest polygon method 22

FIGURE	Page
13 Comparison of ice chart polygon thickness and mean ASPeCt observed thickness in the Ross Sea sector, eliminating data over 2 standard deviations from first order polynomial.....	23
14 Comparison of ice chart polygon thickness and mean ASPeCt observed thickness in the Ross Sea sector, eliminating data over 2 standard deviations from second order polynomial.....	23
15 Map of the study sectors and water depth regimes separated by the dark blue line.....	25
16 Record-length mean annual cycle of sea ice area for the Southern Ocean, the Ross Sector, and the Amundsen/Bellingshausen Sector.....	28
17 Record-length mean annual cycle of sea ice extent for the Southern Ocean, the Ross Sector, and the Amundsen/Bellingshausen Sector.....	29
18 Monthly sea ice area for the Southern Ocean, the Ross Sector, and the Amundsen/Bellingshausen Sector.....	30
19 Monthly sea ice extent for the Southern Ocean, the Ross Sector, and the Amundsen/Bellingshausen Sector.....	31
20 Monthly sea ice area anomaly for the Southern Ocean, the Ross Sector and the Amundsen/Bellingshausen Sector based on the 2000-2009 NIC concentration data.....	33
21 Monthly sea ice extent anomaly for the Southern Ocean, the Ross Sector and the Amundsen/Bellingshausen Sector based on the 2000-2009 NIC concentration data.....	34
22 Length of sea ice growth/decay season determined by the number of days between maximum and minimum sea ice extent for the Southern Ocean, Ross Sector, and Amundsen/Bellingshausen Sector.....	36
23 Monthly percent coverage of total shelf area for the Southern Ocean, Ross Sector, and Amundsen/Bellingshausen Sector.....	38
24 Monthly percent coverage of total oceanic area for the Southern Ocean, Ross Sector, and Amundsen/Bellingshausen Sector.....	39

FIGURE	Page
25 Record-length mean annual cycle of sea ice thickness for the Southern Ocean, the Ross Sector, and the Amundsen/Bellingshausen Sector based on 2000-2009 NIC data	41
26 Monthly sea ice thickness for the Southern Ocean, the Ross Sector, and the Amundsen/Bellingshausen Sector based on NIC data	42
27 Monthly sea ice thickness anomaly for the Southern Ocean, the Ross Sector, and the Amundsen/Bellingshausen Sector based on NIC data	43
28 Record-length mean annual cycle of sea ice volume for the Southern Ocean, the Ross Sector, and the Amundsen/Bellingshausen Sector based on 2000-2009 NIC data	45
29 Monthly sea ice volume for the Southern Ocean, the Ross Sector, and the Amundsen/Bellingshausen Sector based on NIC data	46
30 Monthly sea ice volume anomaly for the Southern Ocean, the Ross Sector, and the Amundsen/Bellingshausen Sector based on NIC data	47
31 ENSO and SAM indices from 2000 through 2010	49
32 Total sea ice concentration anomalies and thickness anomalies in year 2000	50
33 Total sea ice concentration anomalies and thickness anomalies in year 2002	51
34 Total sea ice concentration anomalies and thickness anomalies in year 2008	53

LIST OF TABLES

TABLE		Page
1	Sea ice thickness associated with each stage of development (WMO) in the SIGRID code	16
2	Sea ice concentration in the SIGRID code	17
3	Monthly NIC sea ice extent statistics	26
4	Monthly NIC sea ice area statistics	27
5	Percent variability of NIC extreme sea ice properties during 2000-2009 ..	27
6	Long-term trends of yearly averaged sea ice properties	32
7	Length of sea ice seasons	36
8	Surface area of selected regions	37
9	Monthly NIC sea ice thickness statistics	40
10	Monthly NIC sea ice volume statistics	44

1. INTRODUCTION

While only a small fraction of the global water reservoir is accounted for by sea ice, its impact on Earth's climate and global change is far more dynamical than the response from ice found over the continents. Unlike glaciers and floating ice shelves of terrestrial origin, sea ice is made of frozen seawater. Sea ice is not only much thinner than icebergs calved from terrestrial ice but also more regularly shaped, with a relatively smooth plane level with respect to the sea surface and less freeboard. In contrast continental ice can be up to hundreds of meters thick, is very slow moving and can last for hundreds, even thousands, of years. Some sea ice survives the summer season to become thicker multi-year sea ice, but the vast majority is seasonal and is no more than one meter thick. Thus sea ice variability has immediate impact on the environment.

Sea ice regulates the exchange of heat, moisture and momentum between the ocean and the atmosphere [*Parkinson and Cavalieri, 2008*]. Ice covered areas have much higher albedo than the open ocean surface. Sea ice reflects solar radiation that would otherwise be absorbed by surface waters. It also reduces air-seawater gas exchange dramatically and the net effect of wind stress, depending on concentration and thickness. E.g. sea ice dampens wave activity, which in turn impacts mixing within the seasonal upper layer. Biologically, sea ice is also a sanctuary for wildlife including plankton, algae, penguins, seals, walrus and polar bears.

Southern Ocean sea ice is also important to the global climate for its role in Antarctic Bottom Water (AABW) formation, even though the exact contribution is not well quantified [*Toggweiler and Samuels, 1995; Jacobs, 2004; Dinniman et al., 2007*]. AABW is a key component of the density driven global Meridional Overturning Circulation (MOC). Thus the effects of Antarctic sea ice formation on cold polar surface

This thesis follows the style of *Journal of Geophysical Research*.

waters and their associated freshwater fluxes are crucial to the world's deep ocean circulation [*Jacobs, 2004*].

Sea ice generally forms in high latitude open leads and coastal polynyas, rejecting salt that increases surface water salinity. Extreme winter sea ice formation over certain broad shallow areas around Antarctica produces Shelf Water (SW), the densest water mass in the ocean and a key ingredient of AABW [*Whitworth et al., 1998; Jacobs, 2004; Assmann and Timmermann, 2005*]. Summer melting of sea ice farther offshore produces the local freshening of surface waters within the core of the Antarctic Circumpolar Current (ACC). The strong predominant westerly winds near 60°S push icebergs and sea ice floes to the north, away from the source regions, which results in a net northward freshwater transport.

The top layer of the Southern Ocean must first cool to approximately -1.8°C before sea ice can form. In doing so instability is induced and surface water is replaced from below by slightly warmer and saltier water. Once at the surface freezing point of seawater small crystals form measuring only a few millimeters, also called frazil ice, and reject salt into the surrounding water. This in turn increases surface water salinity and slows sea ice formation. Depending on environmental conditions, the frazil crystals will congeal (Figure 1). In calm conditions, the accumulating frazil crystals form a smooth, thin "film" on the sea surface called grease ice because it resembles an oil slick. The grease ice thickens into sheets called nilas. In rough conditions, the frazil crystals form slush that eventually becomes circular disks with a rough surface called pancake ice [*Comiso and Steffen, 2001*]. Currents and wind push the nilas and pancake ice until their pieces slide on top of each other resulting in rafting. Cementing, congelation and consolidation forms large sheets of sea ice. Over time, pressure squeezes air and impurities out of the sea ice, and under extreme converging pressure the sea ice sheet deforms forming ridges. A ridge (Figure 2) has two main components: the sail, which is visible above the surface, and the keel formed on the underside of the sea ice.

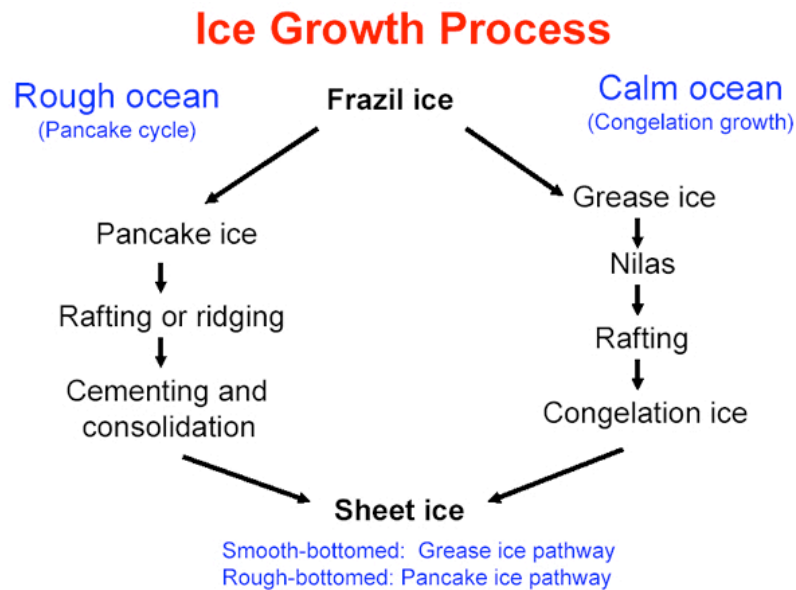


Figure 1. Flow chart depicting the stages of sea ice development, which depends on oceanographic conditions.

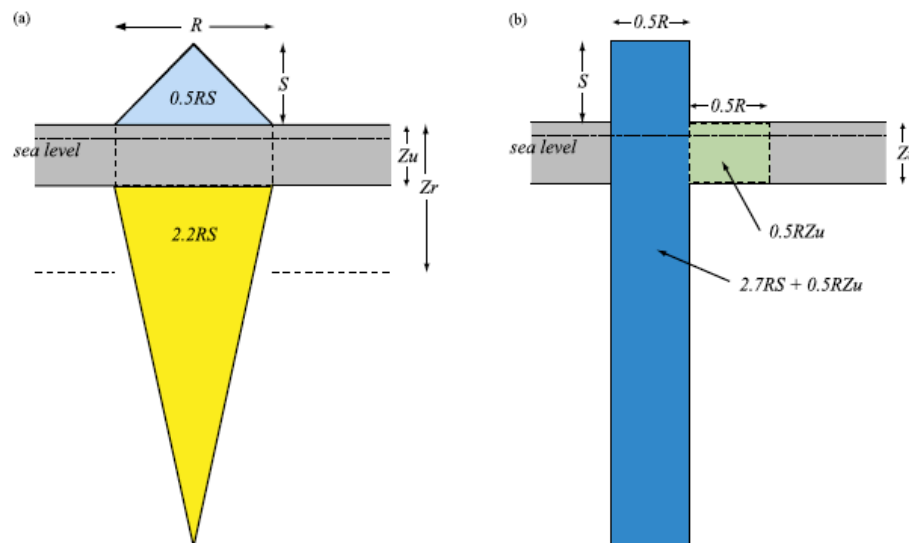


Figure 2. (a) Model ridge and the components where R is the fractional coverage of ridges, S is the average sail height of ridges, Z_u is the average level ice thickness and Z_r is the mean thickness. (b) The numerically modified ridge model used to calculate total thickness. In this case, the ice thickness calculation is no longer a mean thickness, but a value representative of all the different ice types (from *Worby et al. [2008], their Figure 3*).

The harsh environmental conditions at high polar latitudes have always challenged in situ sea ice observations. Sea ice data prior to satellite measurements consists of a sparse collection of observations from early explorers and whalers, but *de la Mare* [1997] suggests that the latter visual records could at least be used to approximate the sea ice edge. Antarctic sea ice extent decreased 25 % from the mid-1950's to the early 1970's [*de la Mare*, 1997], although subject to significant biases in whaling records [*Ackley et al.*, 2003]. More capable vessels and aircraft available by the late 1950's provided scientists with relatively safe and reliable means of accessing and exploring the polar sea ice. During the Arctic Ice Dynamics Joint EXperiment (AIDJEX), 1975-1976, ice camps were set up to conduct long-term studies of sea ice dynamics [*Trowbridge*, 1976]. It was one of the first major studies to examine the dynamical interaction between sea ice, ocean and atmosphere.

It was not until the early 1970's, with the addition of passive microwave sensors to polar orbiting satellites, that our knowledge dramatically expanded on sea ice processes and their connection to ocean circulation and global climate. The first satellite to observe sea ice using an Electrically Scanning Microwave Radiometer (ESMR) was Nimbus 5 in 1972. Nimbus 7 operated with a Scanning Multichannel Microwave Radiometer (SMMR, October 1978 - August 1987). The record was continued by satellites from the Defense Meteorological Satellite Program (DMSP): F8 carried a Special Sensor Microwave/Imager (SSM/I, July 1987 - December 1991), F11 (December 1991 - September 1995) and F13 (May 1995 to present) [*Cavalieri et al.*, 1999; *Cavalieri and Parkinson*, 2008]. Also currently in service are DMSP F15 (since December 1999) and DMSP F17 (since November 2006). An Advanced Microwave Scanning Radiometer-Earth Observing System (AMSR-E) aboard NASA's Aqua satellite has been operational since May 2002. While each of these sensors utilized a different set of frequencies, analyst used their short operational overlap to reconcile differences and to create a continuous time series of sea ice concentration that now spans over three decades [*Cavalieri et al.*, 1999; *Comiso and Steffen*, 2001].

Passive microwave sensors measure the brightness temperature of radiation emitted from the surface of the Earth on nearly a daily basis, regardless of cloud cover or light. Based on that information there are only a couple of algorithms to calculate sea ice concentration as a percentage of surface coverage. An analysis of the differences between sea ice data calculated using the Bootstrap and NASA Team algorithms is detailed in *Comiso and Steffen* [2001]. After over 30 years of continuous sea ice records striking discoveries have been made with respect to air-sea-ice interactions, sea ice variability and inter-decadal trends [*Cavalieri et al.*, 1999; *Comiso and Steffen*, 2001].

Variability of sea ice thickness is relatively unexplored due to the dearth of available in situ observations, and to the lack of a reliable standardization of remotely estimated thickness. Recent attempts include data from satellite-based laser altimetry. Altimeters measure subtle sea surface height anomalies to derive bathymetry but in ice-covered areas they can also detect anomalies due to the freeboard of sea ice, which in turn is approximated to thickness [*Zwally et al.*, 2008]. CryoSat-2 is the first altimeter specifically designed to measure sea ice thickness with a synthetic aperture radar/interferometric radar since April 2010. Instead of a laser it uses powerful pulses of microwaves with improved resolution along-track and across-track of the beam. CryoSat-2 data is not yet publicly available.

Very limited in situ measurements of sea ice thickness have been made using upward-looking sonar (ULS) on naval submarines under the Arctic ice cap [*Kwok and Rothrock*, 2009] and from moored ULS in both hemispheres [*Drinkwater et al.*, 2001; *Fissel et al.*, 2008]. To date, the most accurate measurements of Antarctic sea ice thickness are still derived from direct ship and aircraft observations, but even the most comprehensive compilation is inadequate to study inter-annual to decadal variability [*Worby et al.*, 2008]. Ships operating in or around sea ice generally make hourly records of sea ice concentration, stage of development and floe size of the three predominant types in the vicinity of the vessel. Sea ice thickness, and the height and areal coverage of ridges are

also estimated. A spherical float of known diameter is usually suspended along the side of the ship to aid in estimating sea ice thickness as it breaks and rolls on its side.

Detailed sea ice attributes from satellite data and in situ observations are coded according to the World Meteorological Organization (WMO 1970) standards, using a symbol often referred to as “egg code” due its oval shape (Figure 3). Sea ice concentrations are reported in tenths of coverage of an area with total concentration C_t , and with partial concentrations of the three most predominant sea ice types, from thickest to thinnest sea ice, C_a , C_b , and C_c . Similarly, the corresponding stages of sea ice development in the same area are represented by S_a , S_b , and S_c , and sea ice form or floe size by F_a , F_b , and F_c . Any remaining stages of sea ice older (thicker) than S_a or thinner than S_c are indicated by S_o and S_d . Egg code data is then converted into sea ice gridded (SIGRID) data strings (Figure 4). Only sea ice concentration and stage of development information from the egg code data are used in this study.

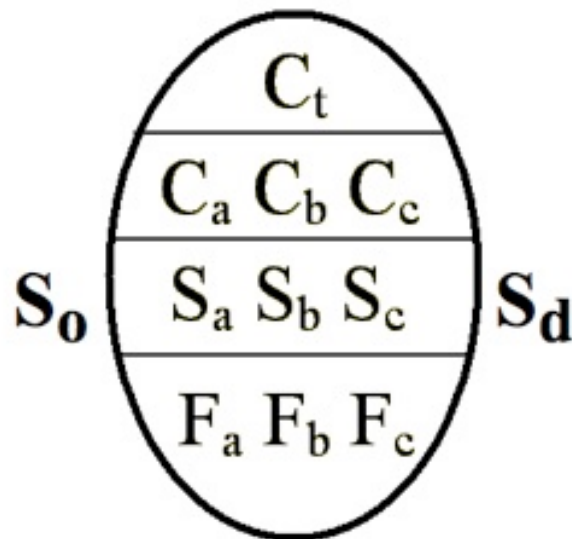


Figure 3. Sample of the World Meteorological Organization (WMO) "egg code" ice reporting protocol.

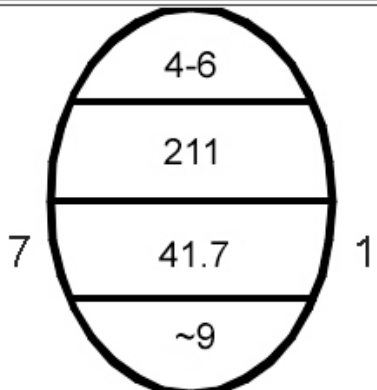
Coding	CTCC CACaCaSaSaFaFa CBCbCbSbSbFbFb CCcCcScScFcFc (CFFpFpFsFs) CNSoSo CDSdSd
Fully Utilized Egg Code	4-6/211/7./4.1.7/1/~9 CC/CaCbCc/So/SaSbSc/Sd/FpFp
Graphical Egg Code	
SIGRID	CT46CA209399CB109199CC108799CF1999CN95CD81

Figure 4. Example of a sample egg code converted to a SIGRID.

1.1 Background

Most recent studies have focused on the dramatic decrease observed in the northern hemisphere sea ice extent, and its relationship to global climate change. *Parkinson et al.* [1999] analyzed passive microwave data in the Arctic from November 1978 to December 1996 and reported a decline in sea ice extent of 34,300 km² annually. *Parkinson and Cavalieri* [2008] extended the study through December 2006 and found a larger decline of 45,100 km² per year, i.e. a 3.7 % loss per decade. Their regional analyses of seasonal and monthly data also revealed negative trends. The interconnectivity of the MOC suggests that these northern climatic changes are bound to eventually impact the Southern Ocean. In a remarkable contrast, however, Antarctic sea ice extent has increased by 11,500 km² annually over the same time period, i.e. about 1.0 %/decade. With the exception of an 8,300 km² yr⁻¹ decrease in the Bellingshausen/Amundsen Seas, all other Antarctic regions experienced increases in sea ice extent over the last 30 years [*Kwok and Comiso, 2002; Zwally et al., 2002; Cavalieri and Parkinson, 2008*].

Large-scale atmospheric variability strongly influences sea ice formation in the Southern Ocean. The Southern Annular Mode (SAM) is the dominant pattern of observed variability represented by variations in the pressure gradient between the Antarctic high-pressure (65°S) and the mid-latitudes (35°S) low-pressure systems, specifically those over New Zealand and the southern Indian Ocean [*Gong and Wang, 1999; Stammerjohn et al., 2008*]. Changes in this pressure gradient are reflected in ocean circulations. ACC transport increases with the stronger westerly winds associated to the positive phase of SAM [*Hall and Visbeck, 2002*], along with increases in surface divergence near the sea ice edge, northward Ekman transport and sea ice extent (Figure 5). The opposite oceanic response is observed during the negative phase of SAM, when weaker westerlies cause reduced sea ice extent.

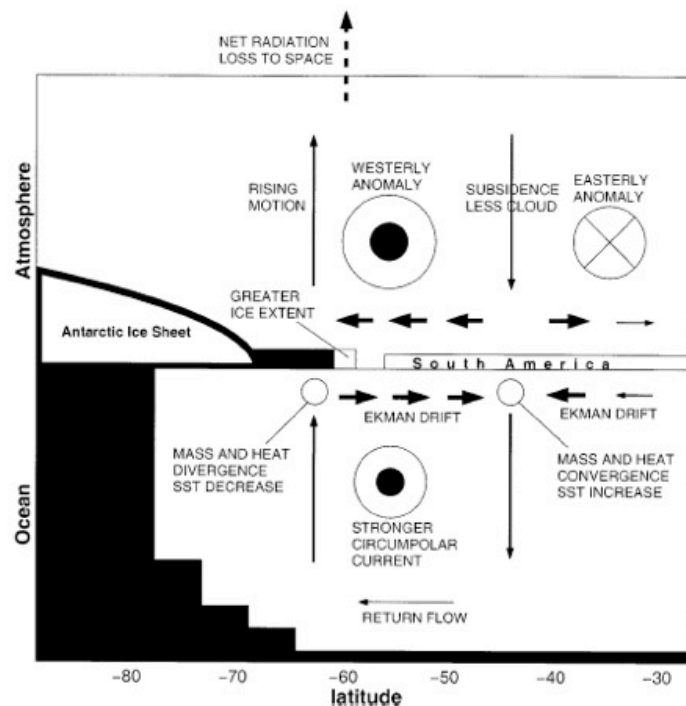


Figure 5. Schematic of positive phase SAM influence on atmospheric and oceanic circulation (from *Hall and Visbeck [2002]*, their Figure 12).

Inter-annual variability in Southern Ocean atmospheric circulation tends to reinforce sea ice extent anomalies. The strengthened atmospheric polar front jet in turn induces a regional dipole (Figure 6), with one polarity located over the west Antarctic Peninsula (WAP) and the southern Bellingshausen Sea, and the other over the western Ross Sea [Kwok and Comiso, 2002; Stammerjohn *et al.*, 2008]. The jet's cyclonic flow anomaly brings colder continental air over the Ross Sea enhancing sea ice formation, and warmer northern air is blown over the Bellingshausen Sea with the opposite effect. During the negative phase of SAM the atmospheric circulation is weakened.

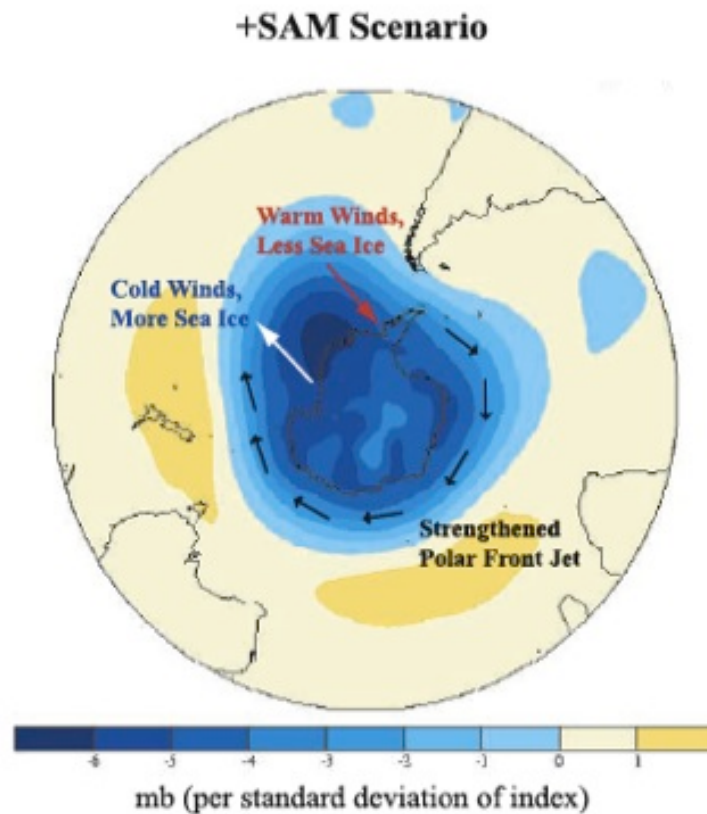


Figure 6. Schematic of a positive SAM phase and impact on sea ice from *Stammerjohn et al.* [2008] (their Figure 1a). The shades of blue represent anomalously low sea level pressure (SLP) while the shades of yellow indicate anomalously high SLP. The black arrows depict the resulting intensified wind circulation while the white and red arrows depict the resulting anomalous sea ice dipole in the Ross Sea and Bellingshausen Sea respectively.

El Niño Southern Oscillation (ENSO) influences the atmospheric subtropical jet in the South Pacific, thus it also modulates the SAM index (Figure 7). During the positive ENSO phase (El Niño), the subtropical jet is strengthened and the polar front is weakened. An anomalous high sea level pressure high over the Amundsen/Bellingshausen Seas promotes higher temperatures/less sea ice formation in the Ross Sea and lower temperatures/more sea ice formation around the Antarctic Peninsula. During the negative phase (La Niña), the polar front is strengthened and the subtropical jet is weakened. An anomalous low sea level pressure over the Amundsen/Bellingshausen Seas has the opposite effect on temperatures and sea ice formation [Yuan, 2004; Yuan and Li, 2008]. Thus, the warming and cooling over the respective dipoles associated to the SAM “seesaw” effect are magnified during La Niña, when the positive phase of SAM coincides with a negative ENSO event, or vice versa, when the negative SAM coincides with a positive ENSO event [Yuan, 2004; Stammerjohn *et al.*, 2008; Yuan and Li, 2008].

A recent study of the seasonal advance and retreat of sea ice revealed noteworthy changes in the duration of the Southern Ocean sea ice cover [Stammerjohn *et al.*, 2008]. The length of the ice season in the western Ross Sea has increased from 1979 to 2004, due to the sea ice northward advance starting about 31 days earlier and its poleward retreat approximately 29 days later. In contrast the sea ice season in the WAP and Bellingshausen Sea for the same time period showed the opposite trend. There sea ice appears to have advanced approximately 54 days later and retreated about 31 days earlier each season. The fact that the total circumpolar sea ice extent shows little variation indicates that the lengthened sea ice season in the western Ross Sea could partially compensate the shortened season in the south Bellingshausen Sea/WAP.

Sea ice in Antarctica is, on average, much thinner (~0.5 m) than in the Arctic (~2 m), and therefore more susceptible to show a more rapid response to global climate change. Also any large-scale steady decline in Southern Ocean sea ice extent could be self-

perpetuating, since even a localized loss enhances atmospheric warming [Parkinson and Cavalieri, 2008]. Retreat of continental glaciers and floating ice shelves in the WAP have already been observed where positive SAM conditions have been favored since the 1990's [Stammerjohn *et al.*, 2008]. Increased regional thermal feedback around the WAP could explain the differing regional 28-year trends in Antarctic sea ice extent noted by Cavalieri and Parkinson [2008], and potentially extend to other regions or even throughout the Southern Ocean.

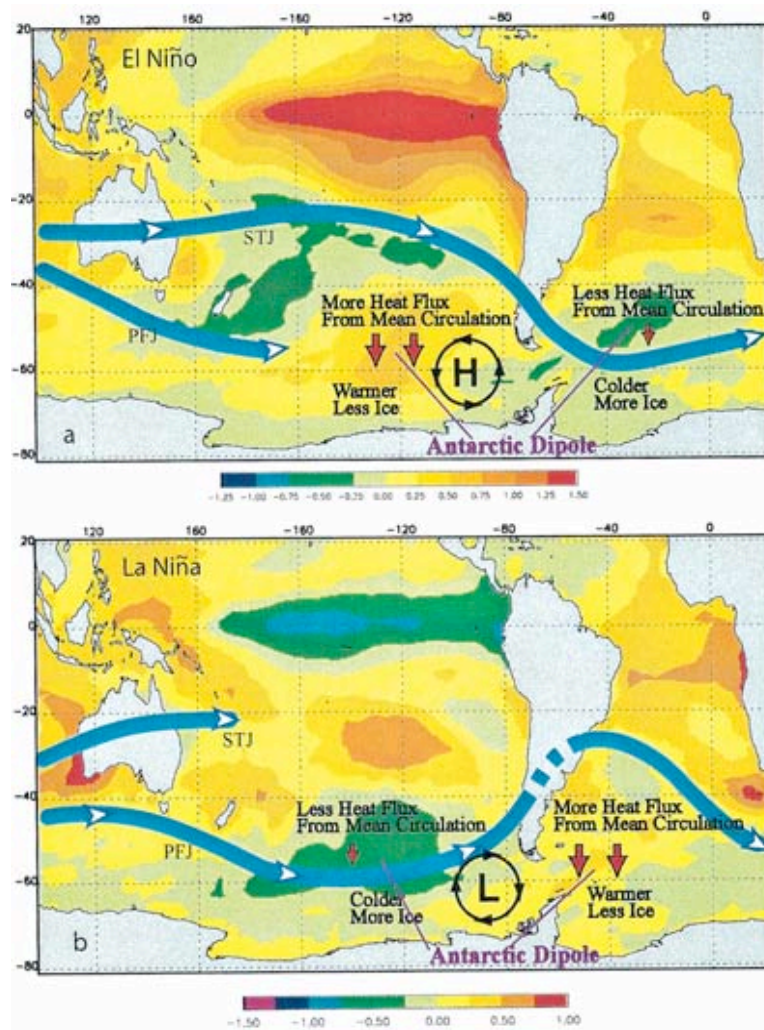


Figure 7. Sea surface temperature anomalies and atmospheric variability associated with (a) the positive phase of the El Niño Southern Oscillation, and (b) the negative phase (from Yuan, 2004, Figure 5).

1.2 Objectives

The primary goal of this study is to create and analyze the first 10-year thickness database for the Southern Ocean utilizing weekly operational sea ice charts produced by the National Ice Center (NIC). The new circumpolar database is inspected for long-term trends and inter-annual variability of hemispheric sea ice properties (extent, area, mean thickness, and volume), and to contrast the patterns of change at key geographic regions (the Ross Sea versus the Amundsen/Bellingshausen Seas) and distinct bathymetric regimes (the shelf versus offshore). To validate the NIC source concentration data, the new time series of sea ice extent and area are compared to time series derived solely from passive microwave data. Similar checks are made with the calculated duration of growth and decay seasons based on the new NIC data.

The contrasting patterns of Arctic and Antarctic sea ice variability imply distinct responses to global climate change. This work describes how these environmental changes manifest in the observed Antarctic sea ice thickness. Among the expected anomalies to be resolved in this study are those associated with well-known atmospheric oscillations like SAM and ENSO. This work will demonstrate the valuable potential of the sea ice thickness proxy to future studies of atmospheric-oceanic interactions. As our understanding of sea ice processes and accuracy of available data improve, so will the importance of understanding the multiple dimensions of ice variability.

2. DATA AND METHODS

2.1 ASPeCt Data

The Antarctic Sea ice Processes and Climate (ASPeCt, www.aspect.aq/data) program was established in 1996 with the objective of compiling all available in situ records of sea ice thickness. The resulting ASPeCt dataset is mainly derived from observations on research vessels and icebreakers from Australia, Great Britain, Germany, United States and Russia; and some observations on helicopters.

According to ASPeCt protocols, observations are generally recorded hourly and should characterize the three most predominant of the various ice conditions observed within 1 km of the vessel [Worby *et al.*, 2008]. In this study the ice attributes used for each ASPeCt observation is the average of the three reported ice types. The complete data set consists of 23,373 observations from 1980 through 2005 (Figure 8). To avoid spatial bias a subset of 14,557 observations is also available, in which observation within 6 nautical miles of the previous data point were eliminated on the assumption that a vessel transits at approximately 6 knots through level ice.

The estimated mean ice thickness (T_{mean}) for each ASPeCt observation [Deliberty *et al.*, 2004; Worby *et al.*, 2008] is calculated as the sum of level ice thickness, and equivalent ridged ice thickness. For observations that include data on level ice (Z_u), areal percentage of ridges (R) and average sail height of ridges (S) Worby *et al.* [2008] developed simple geometrical models for the mean sea ice thickness that takes into account the contribution of ridges according to Figure 2. This relatively simple calculation takes into account the various ice conditions that might exist within a 1 km radius.

2.2 NIC Data

The NIC is a collaborative organization between the National Oceanic and Atmospheric Administration (NOAA), the U.S. Navy, and the U.S. Coast Guard with the goal of providing “the highest quality, timely, accurate, and relevant snow and ice products and services to meet the strategic, operations, and tactical requirements of the United States interests across the global area of responsibility” (www.natice.noaa.gov). The NIC has been collecting and mapping ice data in the southern hemisphere since the early 1970’s in the interest of safe navigation [*DeLiberty et al.*, 2004; *Tang and Wong*, 2008]. Analysts use information obtained from ship observations, aircraft reconnaissance, infrared imagery, meteorological and oceanographic models, SAR, and the passive microwave imagery to ascertain current sea ice conditions. All of these compiled data are spatially grouped into polygons with similar sea ice conditions (Figure 9). Each

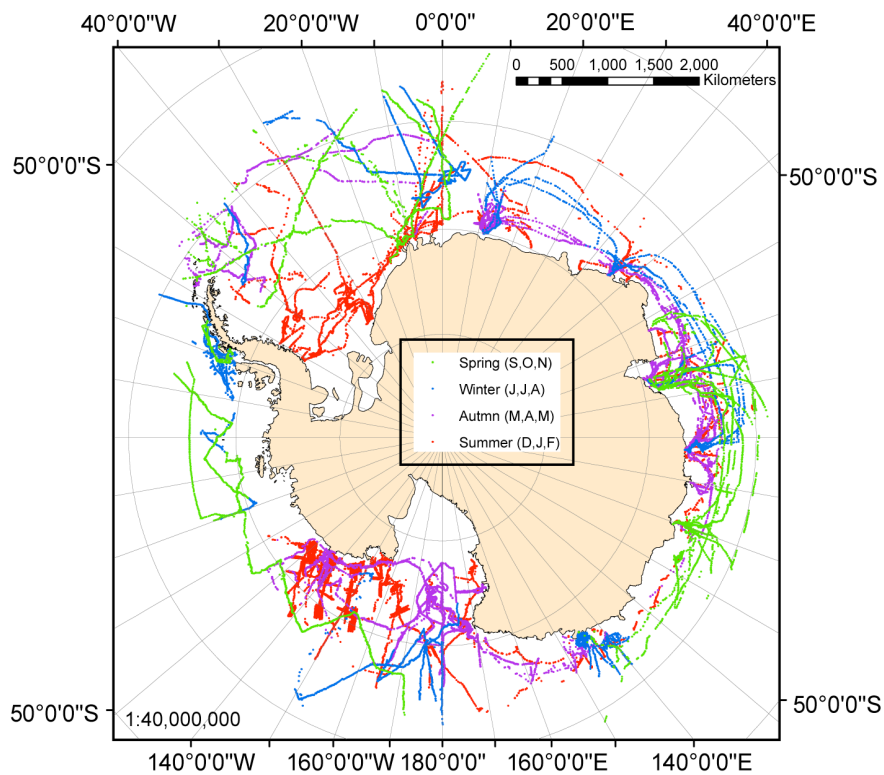


Figure 8. Geographic representation of all ASPeCt observations. Each dot represents an ice thickness observation, and color the Austral season the observation was recorded in. (after *Worby et al.* [2008], Figure 1).

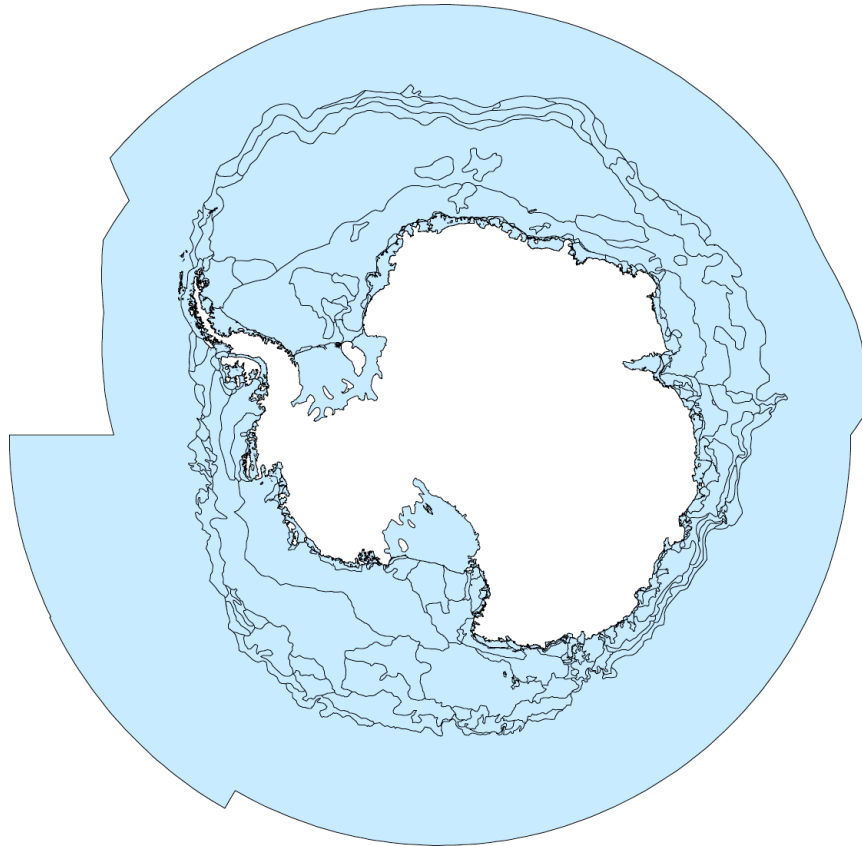


Figure 9. Example of NIC weekly ice chart polygons from November 2000. Each polygon represents similar ice conditions. The polygons are updated weekly to reflect the changing ice conditions.

polygon contains a SIGRID string of sea ice data as illustrated in Figure 4. SIGRID information in the NIC ice data is used as a proxy for sea ice thickness [Deliberty *et al.*, 2004]. The estimated sea ice thickness for each NIC polygon is based on the stage of development (S_a , S_b , S_c , Table 1) and concentration (C_a , C_b , C_c , Table 2) data, calculated as:

$$T_{NIC} = \left(\frac{C_a}{10}\right)S_a + \left(\frac{C_b}{10}\right)S_b + \left(\frac{C_c}{10}\right)S_c$$

This sea ice thickness proxy has previously been validated with spatially and temporally overlapping measurements made by the ASPeCt program in the Ross Sea between 1995 and 1998 [DeLiberty *et al.*, 2004]. Thus it has potential value toward creating a weekly time series with complete polar coverage.

Table 1. Sea ice thickness associated with each stage of development (WMO) in the SIGRID code.

Thickness (S_a , S_b , S_c)			
Median (cm)	(+/- cm)	Stage of Development	SIGRID Code
0	0	Ice Free	00
5	5	New Ice (<10 cm: Pack, Slush, Shuga)	81
5	5	Nilas (<10 cm)	82
12.5	2.5	Grey Ice (10-15 cm)	84
20	10	Young Ice (10-30 cm)	83
22.5	7.5	Grey-White Ice (15-30 cm)	85
50	20	White Ice (30-70 cm)	87
95	25	First-Year Medium (70-120 cm)	91
115	85	First-Year Ice (30-200 cm)	86
160	40	First-Year Thick (>120 cm)	93
160	40	Old Ice (gone thru one summer)	95
100	100	Land-Fast Ice	08
999	999	No Data	80,98,99

2.3 Quality Control of NIC Data

There are several challenging inconsistencies in the NIC ice data. The temporal frequency of the source charts was not the same throughout the study period. Originally, Southern Ocean ice charts were produced weekly, but starting in 2001 the NIC reduced their output to every other week due to personnel reductions. There were NIC data reported as “not observed”, and presumably not existent.

Table 2. Sea ice concentration in the SIGRID code.

Concentration (C_t, C_a, C_b, C_c)		
Definition	Code	Value
Ice Free	00	0
< 1/10	01	0.5
Bergy Water	02	0
1/10	10	1
2/10	20	2
3/10	30	3
4/10	40	4
5/10	50	5
6/10	60	6
7/10	70	7
8/10	80	8
9/10	90	9
>9/10, <10/10	91	9.5
10/10	92	10
Intervals		
1/10 - 3/10	13	2
4/10 - 6/10	46	5
7/10 - 9/10	79	8
9/10 - 10/10	91	9.5
Unknown	99	

Although every polygon has a finite total concentration (C_t), but occasionally some of the partial concentrations (C_a , C_b , and C_c) were missing in the NIC data files, which they report as “no data”. Missing partial concentration data fall into three different scenarios: (1) a finite C_t , but missing C_a , C_b and C_c ; (2) a finite C_t and one of the three partial concentrations, but missing the other two partial concentrations (e.g. C_b and C_c); and (3) a finite C_t and two of the three partial concentrations, but missing the third partial concentration (e.g. C_c). Assuming the sum of all three partial concentrations equals C_t , for the third scenario, the single missing value is easily recovered from C_t . Scenarios with more than one missing partial concentration are filled in with the corresponding 2000-2005 record-length average partial concentration.

2.4 Source Data Errors

The error associated with the ASPeCt data diminishes with increasing thickness of the observed floe: $\pm 50\%$ for ice thinner than 0.1 m, $\pm 30\%$ for ice between 0.1 m and 0.3 m and $\pm 20\%$ for level ice thicker than 0.3 m. These errors are based on regular comparison of observations with actual drilled measurement of ice thickness [Worby *et al.*, 2008].

Similarly the errors associated with the ice thickness proxy derived from NIC stage of development data depend on the range of thickness assigned to each stage (Table 1). For example, a mean of 22.5 cm with an error of ± 7.5 cm is estimated for gray-white ice that normally varies between 15 cm and 30 cm. Also the sea ice concentration total error is $\pm 10\%$ of the range of thickness. Thus the ice thickness error for a given NIC polygon could at most be the cumulative error from three different types of ice.

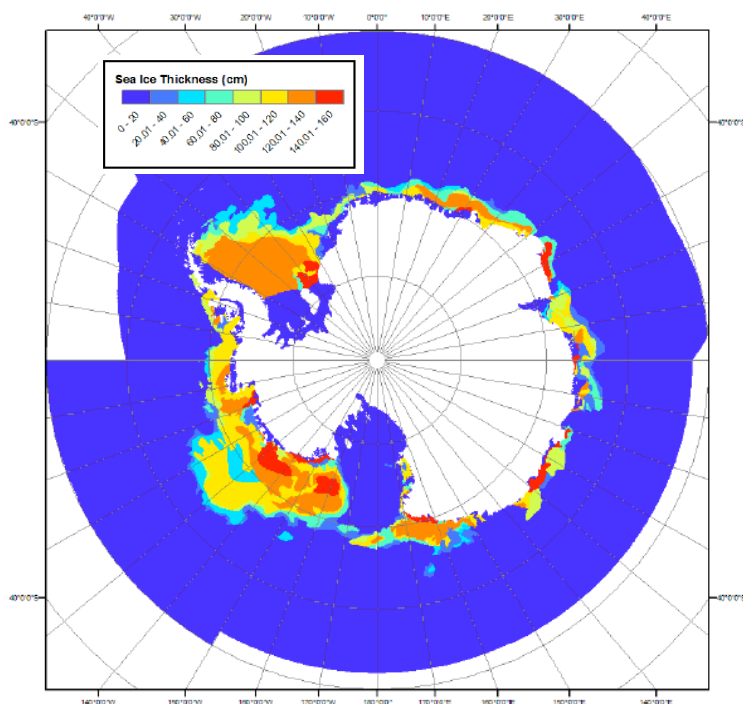


Figure 10. Example weekly ice chart displaying calculated ice thickness values for 04-10 January 2000.

2.5 Gridded NIC Data

NIC adopted the Geographic Information Systems working file format, called “shapefile”, to facilitate the previewing of polygons and attributes of weekly hemispheric data (Figure 10). NIC source data is exported to a non-projected World Geodetic Survey 1984 Geographic Coordinate System, before its mapping onto a uniform 15 km x 15 km grid for the circumpolar region from 30°S to 80°S created in Albers Polar Stereographic equal-area projection. Thus source NIC polygon data are assigned to each grid point, i.e. total sea ice concentration and thickness values based on the grid’s enclosing polygon. The new gridded sea ice data are “stacked” chronologically. In the few cases where weekly ice charts had missing data for certain polygons the corresponding grid point values were interpolated in time. Finally the stacked gridded NIC data is temporally interpolated to exactly seven-day intervals over the full length of the time series.

3. DATA COMPARISON

ASPeCt observations of sea ice thickness are used to ground truth the NIC proxy of total ice thickness. Note, however, that the two data sets only overlap in 2000-2005. The proxy for NIC data does not resolve thicknesses greater than 160 cm, which is the thickest mean value assigned to any of the stages of development. Thus all ASPeCt values greater than 160 cm were eliminated prior to the comparison. Two different methods are used to compare the two data sets. The first method compares the average thickness of all concurrent, or closest in time, ASPeCt observations within the same NIC polygon [DeLiberty *et al.*, 2004]. By using the median ASPeCt thickness the difference in the goodness of fit was minimal. The second method compares the nearest NIC polygon to every single ASPeCt thickness observation. Temporal comparisons are made by year, month and season, whereas spatial comparisons by hemisphere, sector and region.

Polynomial fits to scatter plots with all the corresponding thickness comparison points are calculated via an iterative elimination method. All data outside a specified number of standard deviations (2, 2.5, and 2.8) from a polynomial fit are eliminated before proceeding with the fit to the remaining data points, until no outliers are found. First and second order polynomials are used for the fits. In theory the observed ice thickness would equal the ice thickness calculated by proxy, a linear relationship as in DeLiberty *et al.* [2004]. However, the use of second order polynomial fits is justified by the much wider range of ice thickness associated with first year and older ice than younger thinner ice stages. Thus it is assumed that the relationship between the two data sets could potentially change as the ice matures.

Goodness of fit is a correlation coefficient (R) representing how well two variables covary in time or space, where $R = 0$ means the points are randomly scattered and $R = 1$ means the points are in total correlation [Emery and Thomson, 2001]. Overall, the

goodness of the linear fit to the two data sets was poor ($R \leq 0.4$) compared to *DeLiberty et al.* [2004] fit ($R = 0.77$) of data from May/June 1995, August 1995 and May/June 1998 in the Ross Sea sector. When the iterative elimination method is applied, the goodness of fit can be improved, but is highly variable (between $R = 0.10$ and $R = 0.92$). The localized scale of the direct observations offered considerable variability compared to the generally larger scale of the ice thickness proxy based on stage of development. Thus the second order polynomial fit usually produced a slightly higher goodness of fit.

The validity of the comparisons is limited by the amount of data being compared. The vast majority of the ASPeCt ice thickness observations were recorded during the austral summer months, followed by the spring and fall seasons, with a relatively small amount collected in the austral winter months. The observations are unevenly distributed spatially as well. Large clusters of ASPeCt observations are located in the Ross Sea and around the Antarctic Peninsula, in the vicinity of research bases, while the areas in between are only sporadically sampled. In cases with only a small number of comparison points, a high goodness of fit is achieved by eliminating just a couple data points (Figure 11). However, this data subset cannot reasonably be considered representative of the entire hemispheric conditions. Conversely, the higher variability associated with larger amounts of data points (Figure 12) usually result in a lower goodness of fit. In either case, data points eliminated as “outliers” using the iterative elimination method could potentially be valid data.

The nearest polygon method of comparing the data proved to be of little value (Figure 12). These results show that a wide range of thickness observations are contained within a single polygon, producing “columns” that make reliable polynomial fitting ambiguous. Of all the comparisons made in this study, those for the Ross Sea in the austral summer months data is considered the most reliable. This region/season has the highest number of ASPeCt observations and the Ross Sea provides relatively low

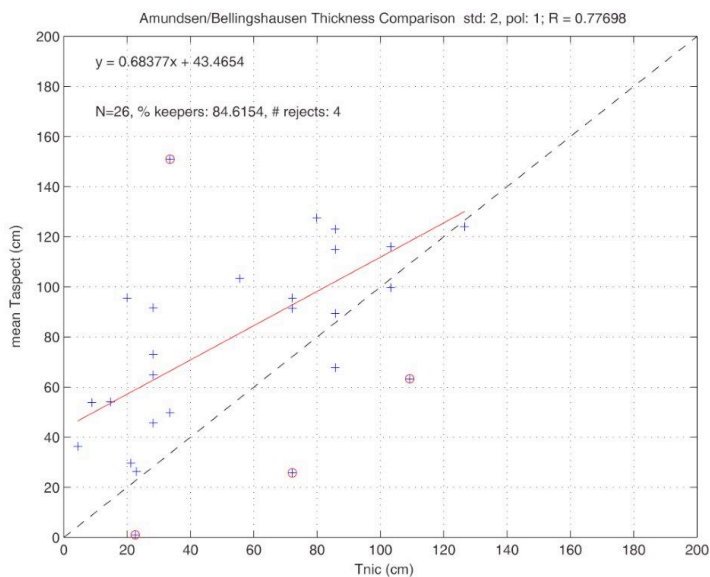


Figure 11. Comparison of ice chart polygon thickness (Tnic) and mean ASPeCt observed thickness (Taspect) in the Amundsen/Bellingshausen sector demonstrating a relatively high goodness of fit with relatively few data points. The red circles are data excluded via the iterative elimination method.

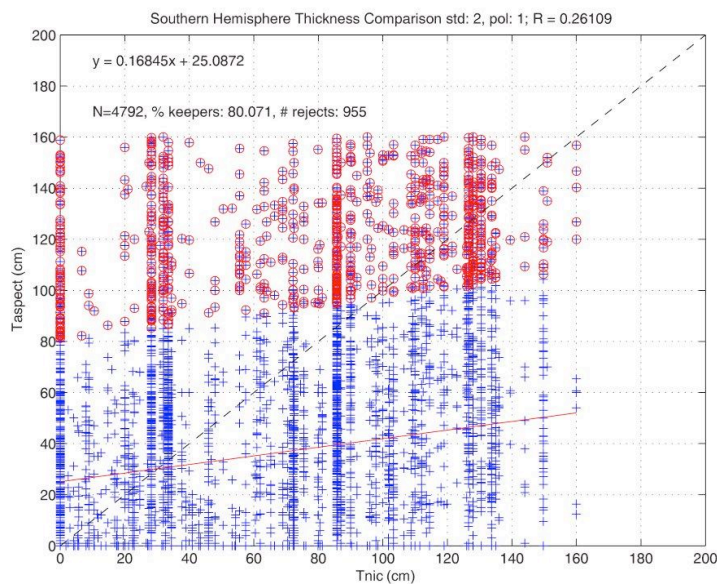


Figure 12. Comparison of southern hemisphere ice thickness using the nearest polygon method. The red circles are data excluded via the iterative elimination method.

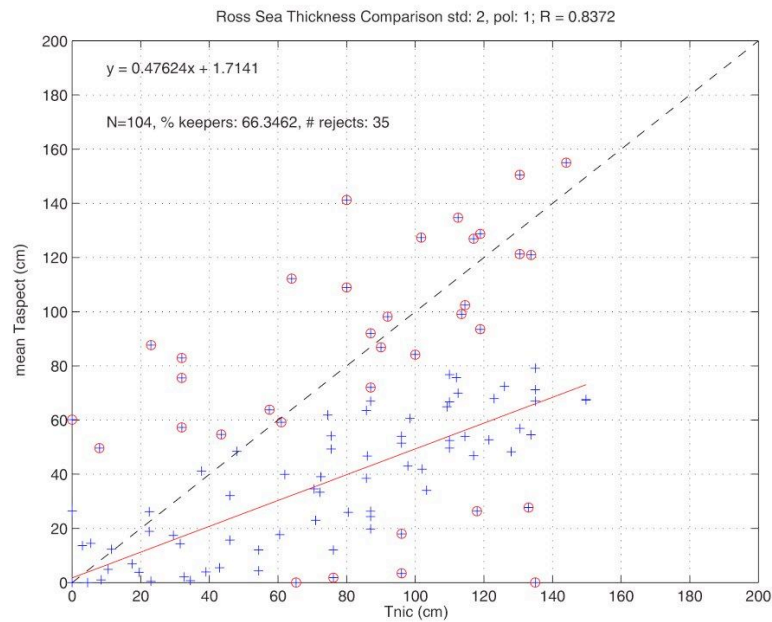


Figure 13. Comparison of ice chart polygon thickness (Tnic) and mean ASPECT observed thickness (Taspect) in the Ross Sea sector, eliminating data over 2 standard deviations from first order polynomial. The red circles are data excluded via the iterative elimination method.

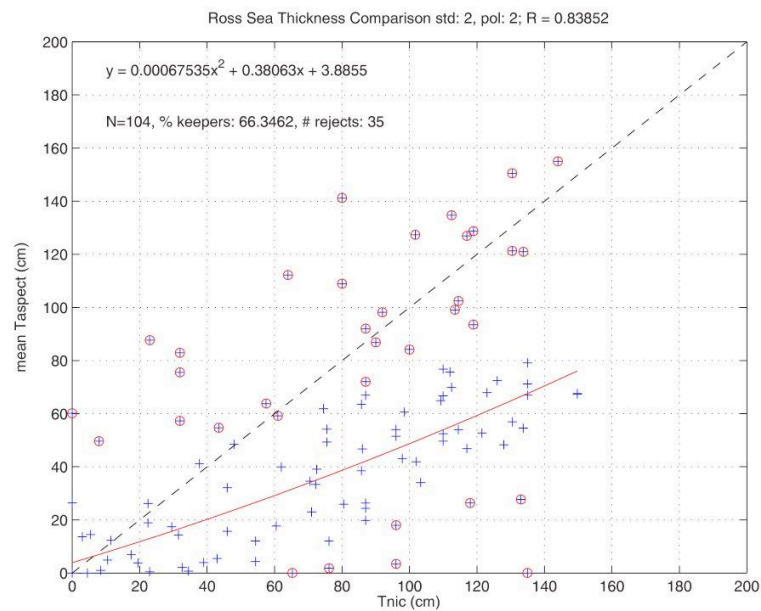


Figure 14. Comparison of ice chart polygon thickness (Tnic) and mean ASPECT observed thickness (Taspect) in the Ross Sea sector, eliminating data over 2 standard deviations from second order polynomial. The red circles are data excluded via the iterative elimination method.

variability in sea ice thickness during this time: most of the thinner annual ice melts and the majority of the ice that remains is thicker multi-year ice. There are 104 comparison data points within the Ross Sea sector, with 35 outside two standard deviations from the linear trend, and a resulting goodness of fit of $R = 0.837$ (Figure 13). Using a second order polynomial also eliminates 35 data points but it renders a slightly higher $R = 0.839$ (Figure 14). These results show that the NIC ice data over-estimate the ASPeCt ice thickness observations by nearly 50 percent. Expanding to two standard deviations exclusion eliminates 2 data points and reduces the goodness of fit to $R = 0.58$.

The highly variable ice conditions contained within the NIC polygons make pin-pointing an “optimal proxy correction” unreasonable. Ships operating in or near ice tend to seek out the path of least resistance, which does bias the ASPeCt data toward thinner ice. Ship activity in the Southern Ocean is also highly biased toward the austral summer months. The ASPeCt observations have a resolution of 1 km, whereas data from the NIC polygons encompass areas that range from a few km^2 to thousands of km^2 . The NIC stage of development proxy does not account for ridging, deformation of older ice, nor snow cover, therefore rendering thinner ice than ASPeCt observation would in many cases. Furthermore, the NIC thickness proxy becomes less reliable with older ice, as the potential range of thickness increases. A closer examination of this disparity revealed a change in the stage of development classification. During the 1995-1998 period studied by *DeLiberty et al.* [2004] the NIC divided “first year ice” into five bins, but later the classification was reduced to three bins. This change in protocol reduces the resolution of older, thicker ice.

Ground truth of NIC weekly sea ice data with in situ observations is crucial, but the quality and consistency of NIC protocols must first improve. Standardized in situ sea ice thickness observations are continuously added to the ASPeCt database. Therefore comparisons of the kind shown here may produce slightly improved correlations in the future with the advent of new remote sensing technologies.

4. ANALYSIS AND RESULTS

Two regions are selected in this study of sea ice properties to explore the influence of dominant atmosphere-induced inter-annual variability. We define the Ross Sea sector as extending from 160°E to 130°W and the Amundsen/Bellingshausen sector from 130°W to 75°W (Figure 15). Sea ice properties are also contrasted between the shelf and the oceanic regimes, defined as regions inshore (offshore) of the 1000-m isobath at the continental slope.

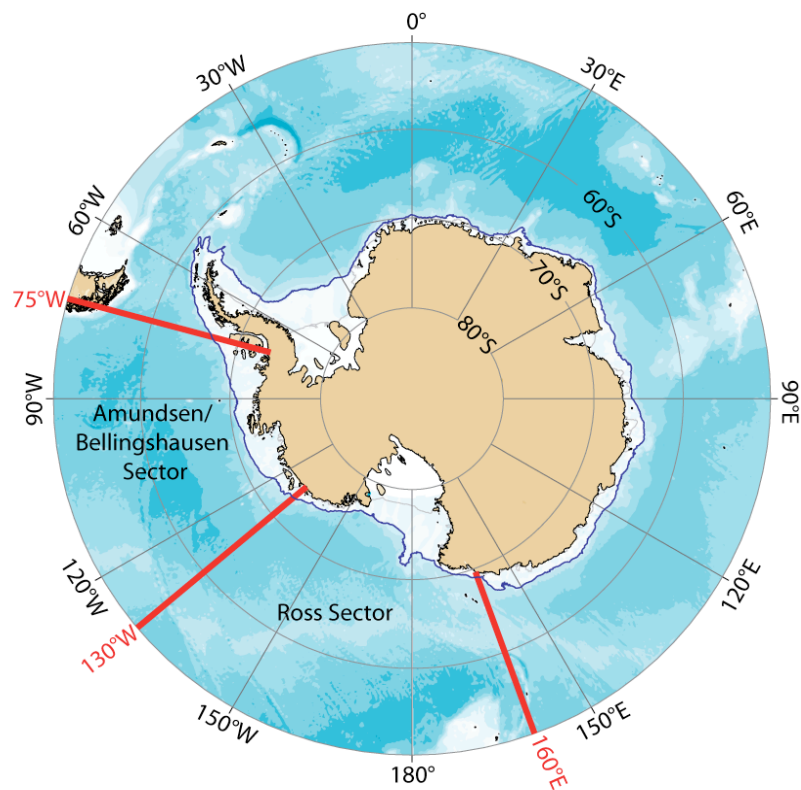


Figure 15. Map of the study sectors and water depth regimes separated by the dark blue line (1000-m isobaths).

4.1 Sea Ice Extent and Area: Decadal and Inter-annual Variability

Sea ice extent for a given region is calculated as the sum of all grid point areas (15 km x 15 km) with an ice concentration $\geq 15\%$. The 15% threshold is generally used in sea ice extent studies because passive microwave sensors have difficulty differentiating between thin ice and water at concentrations lower than approximately 10%. Unlike extent, sea ice area is the actual portion of the sea surface covered by ice regardless of its concentration, i.e. the grid point area (225 km²) times concentration.

The record-length mean (2000-2009) annual cycle for the Southern Ocean sea ice area and extent are calculated from the new NIC data and shown as blue curves in Figures 16a and 17a. They reveal minima in February, expanding for seven months to reach a maximum in September before decaying for five months. The corresponding record-length mean (2000-2007) annual cycles derived from passive microwave data (green curves) are very similar. The monthly time series of Southern Ocean sea ice area and extent (blue curves in Figures 18 and 19; Tables 3 and 4) show clear sinusoidal-like seasonality with little inter-annual variability, in close agreement with the passive microwave time series [Zwally *et al.*, 2002; Cavalieri and Parkinson, 2008]. Inspection of extreme conditions in the NIC time series (Table 5) indicate that February's minimum area (extent) varied by 38.2% (37.2%) and September's maximum by only 8.1% (5.1%).

Table 3. Monthly NIC sea ice extent statistics.

EXTENT	Mean	Maximum		Minimum	
		month-year	10 ⁶ km ²	month-year	10 ⁶ km ²
Southern Ocean	11.40	Sep-09	17.60	Feb-06	3.00
Ross	2.83	Sep-07	4.38	Feb-06	0.61
Amundsen/Bellingshausen	1.19	Sep-07	2.02	Feb-06	0.32

Table 4. Monthly NIC sea ice area statistics.

AREA	Mean 10 ⁶ km ²	Maximum		Minimum	
		month-year	10 ⁶ km ²	month-year	10 ⁶ km ²
Southern Ocean	9.64	Sep-09	15.80	Feb-00	2.17
Ross	2.43	Sep-07	3.97	Feb-06	0.04
Amundsen/Bellingshausen	0.98	Oct-09	1.75	Feb-03	0.22

Almost identical patterns of record-length mean annual cycles (Figures 16 and 17) and monthly time series (Figures 18 and 19) are observed in both the Ross and the Amundsen/Bellingshausen sectors, albeit their regional extreme conditions showed at least twice as much temporal variability than for the entire Southern Ocean (Table 5). The presence of massive grounded icebergs also had an impact on the local circulation and sea ice production over some shelf areas, i.e. giving rise to multiple peaks during the austral winter months.

Table 5. Percent variability of NIC extreme sea ice properties during 2000-2009.

Variability (%)	Minimum		Maximum	
	Month	Range	Month	Range
Extent				
Southern Ocean	Feb	37.2	Sep	5.1
Ross	Feb	64.7	Sep	25.4
Amundsen/Bellingshausen	Feb	64.2	Sep	43.0
Area				
Southern Ocean	Feb	38.2	Sep	8.1
Ross	Feb	74.7	Sep	29.8
Amundsen/Bellingshausen	Feb	73.2	Sep	44.1
Thickness				
Southern Ocean	May	41.4	Dec	36.7
Ross	Apr	72.0	Dec	52.9
Amundsen/Bellingshausen	May	68.0	Jan	53.3
Volume				
Southern Ocean	Mar	78.5	Nov	66.7
Ross	Mar	96.9	Oct	69.9
Amundsen/Bellingshausen	Mar	109.7	Nov	90.7

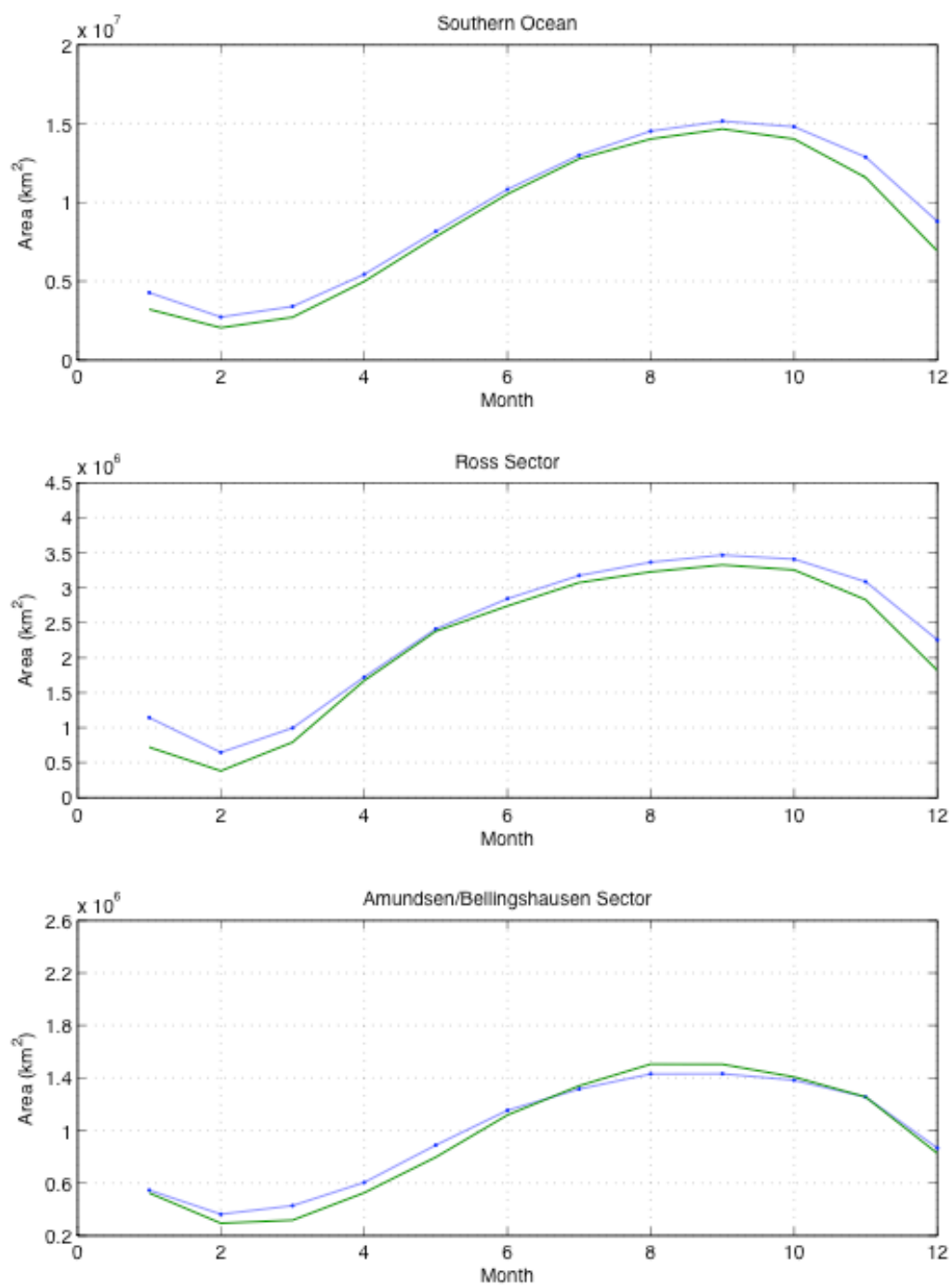


Figure 16. Record-length mean annual cycle of sea ice area (km²) for the Southern Ocean (top), the Ross Sector (middle), and the Amundsen/Bellingshausen Sector (bottom). The blue (green) curves is computed based on the 2000-2009 NIC (2000-2007 passive microwave) concentration data.

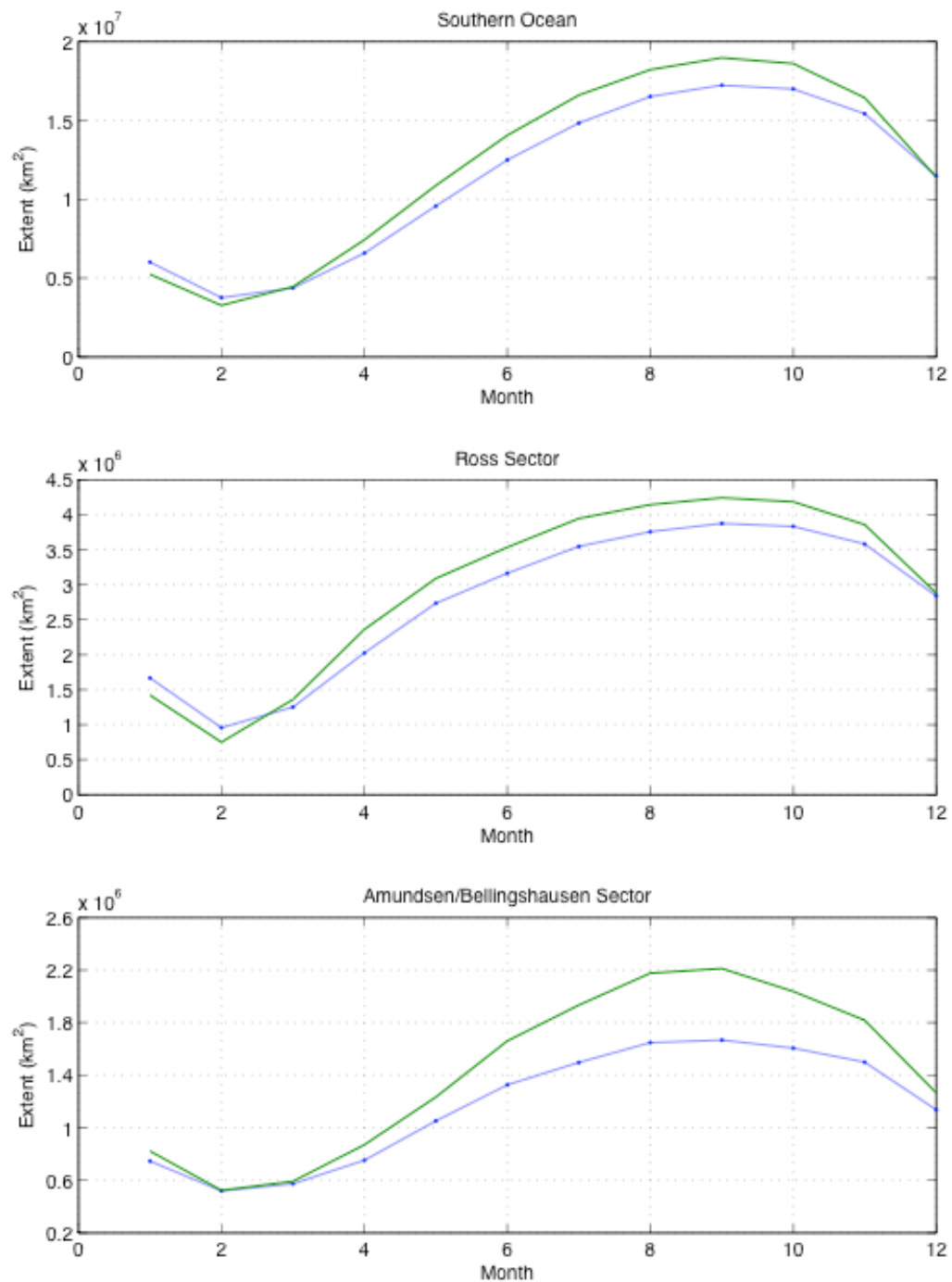


Figure 17. Record-length mean annual cycle of sea ice extent (km²) for the Southern Ocean (top), the Ross Sector (middle), and the Amundsen/Bellinghshausen Sector (bottom). The blue (green) curve is computed based on the 2000-2009 NIC (2000-2007 passive microwave) concentration data.

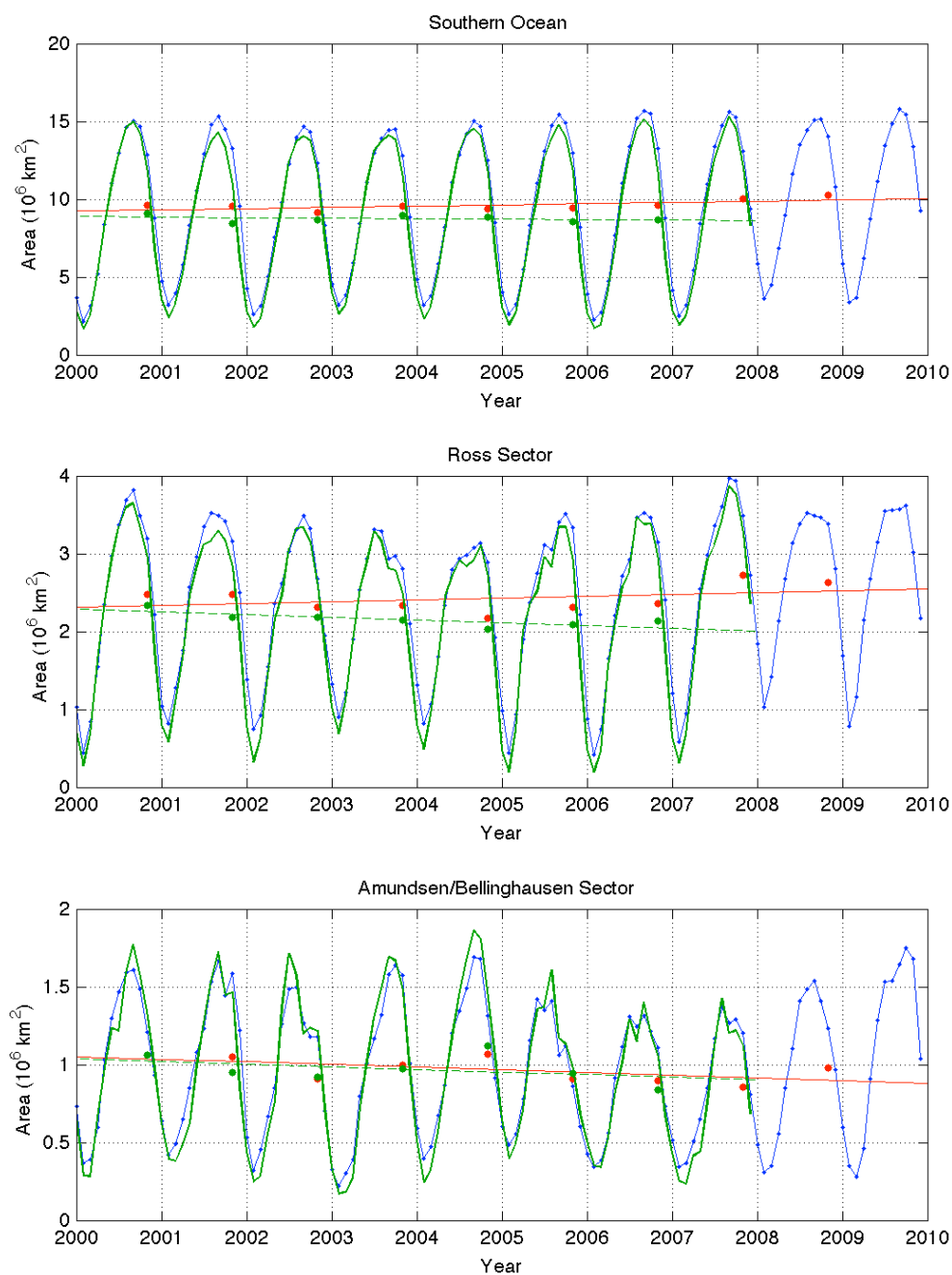


Figure 18. Monthly sea ice area (10^6 km^2) for the Southern Ocean (top), the Ross Sector (middle), and the Amundsen/Bellinghausen Sector (bottom). The blue (green) curve is computed based on the 2000-2009 NIC (2000-2007 NSIDC passive microwave) concentration data; the red (green) line is the linear fit to yearly-averaged NIC (NSIDC) data (red and green dots).

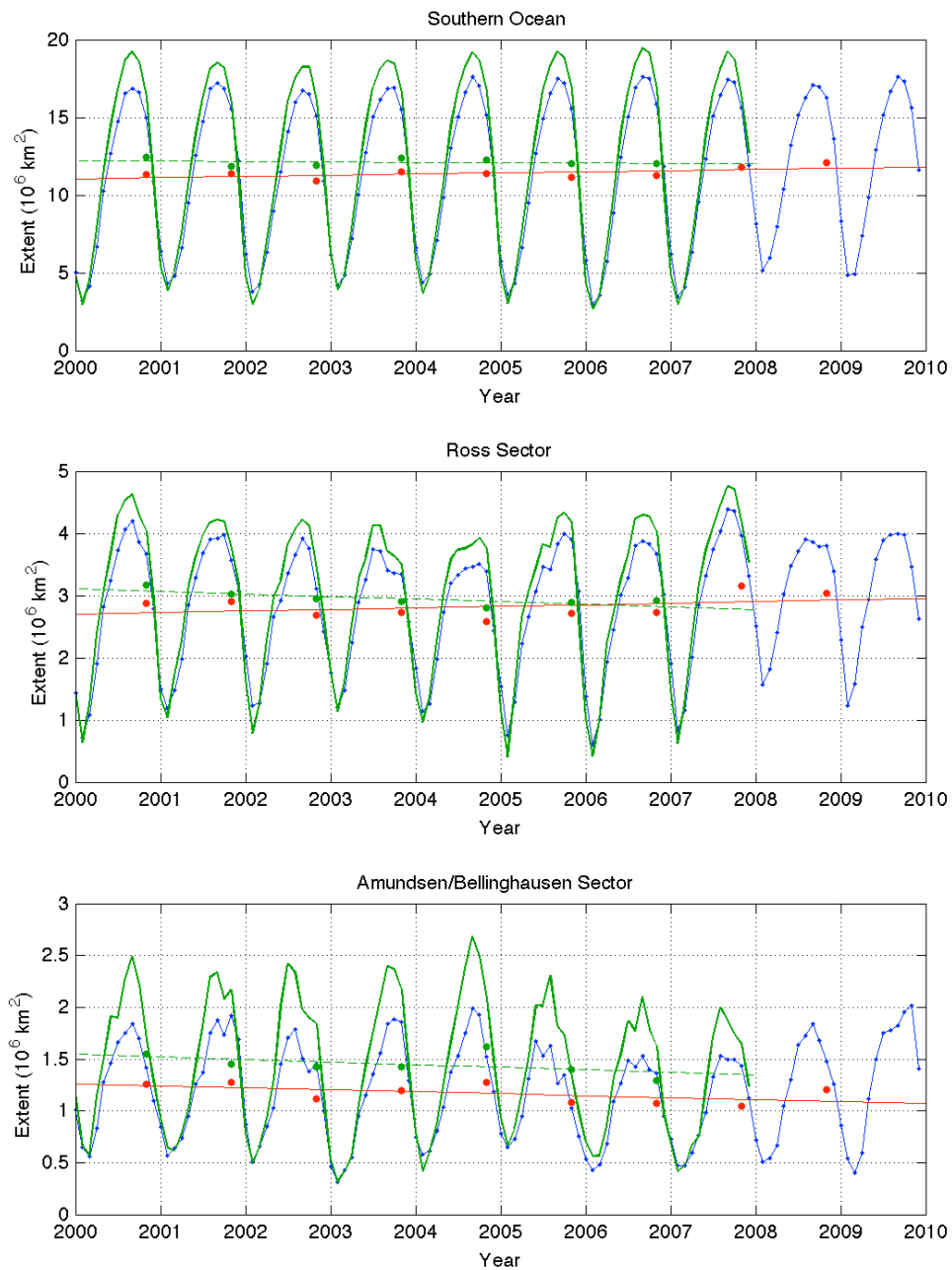


Figure 19. Monthly sea ice extent (10^6 km^2) for the Southern Ocean (top), the Ross Sector (middle), and the Amundsen/Bellinghausen Sector (bottom). The blue (green) curve is computed based on the 2000-2009 NIC (2000-2007 NSIDC passive microwave) concentration data; the red (green) line is the linear fit to yearly-averaged NIC (NSIDC) data (red and green dots).

Table 6. Long-term trends of yearly averaged sea ice properties.

	(2000-2007)		(2000-2009)	
	NSIDC	NIC	NIC	
	% change/decade		change/decade	% change/decade
AREA				
Southern Ocean	-3.2	-0.6	$0.71 \times 10^6 \text{ km}^2$	7.7
Ross	-13.2	-10.8	$0.21 \times 10^6 \text{ km}^2$	9.1
Amundsen/Bellingshausen	-14.2	-18.1	$-0.15 \times 10^6 \text{ km}^2$	-14.6
EXTENT				
Southern Ocean	-1.7	-0.1	$0.70 \times 10^6 \text{ km}^2$	6.3
Ross	-11.7	-9.4	$0.23 \times 10^6 \text{ km}^2$	8.5
Amundsen/Bellingshausen	-14.4	-19.2	$-0.17 \times 10^6 \text{ km}^2$	-13.4
THICKNESS				
Southern Ocean			22.6	49.2
Ross			23.8	47.0
Amundsen/Bellingshausen			20.7	44.8
VOLUME				
Southern Ocean			$3.78 \times 10^3 \text{ km}^3$	68.3
Ross			$1.11 \times 10^3 \text{ km}^3$	75.8
Amundsen/Bellingshausen			$0.17 \times 10^3 \text{ km}^3$	26.0

Southern Ocean sea ice area (extent) increased (Table 6) at a rate of 7.7 %/decade (6.3 %/decade), or $0.71 \times 10^6 \text{ km}^2/\text{decade}$ ($0.70 \times 10^6 \text{ km}^2/\text{decade}$), as indicated by the linear fits (red lines) to the NIC yearly mean 2000-2009 values shown as red dots in Figures 18 and 19. Approximately the same trends of increase are estimated for the Ross Sea: an increase rate of 9.1 %/decade (8.5 %/decade), or $0.21 \times 10^6 \text{ km}^2/\text{decade}$ ($0.23 \times 10^6 \text{ km}^2/\text{decade}$). However, the Amundsen/Bellingshausen sector shows the opposite trend and with a significantly larger percentage change: a decrease of -14.6 %/decade (-13.4 %/decade), or $-0.15 \times 10^6 \text{ km}^2/\text{decade}$ ($-0.17 \times 10^6 \text{ km}^2/\text{decade}$).

Table 6 shows the remarkable difference that the last couple (2008-2009) of years of NIC data make on these trends. When trends are computed just for the 2000-2007 period, there is an overall agreement among all of the decreasing yearly rates in sea ice area and extent derived from either yearly averaged passive microwave (green dots) or NIC (red dots) data (Figures 18-19). Extending the NIC time series to 2009 was

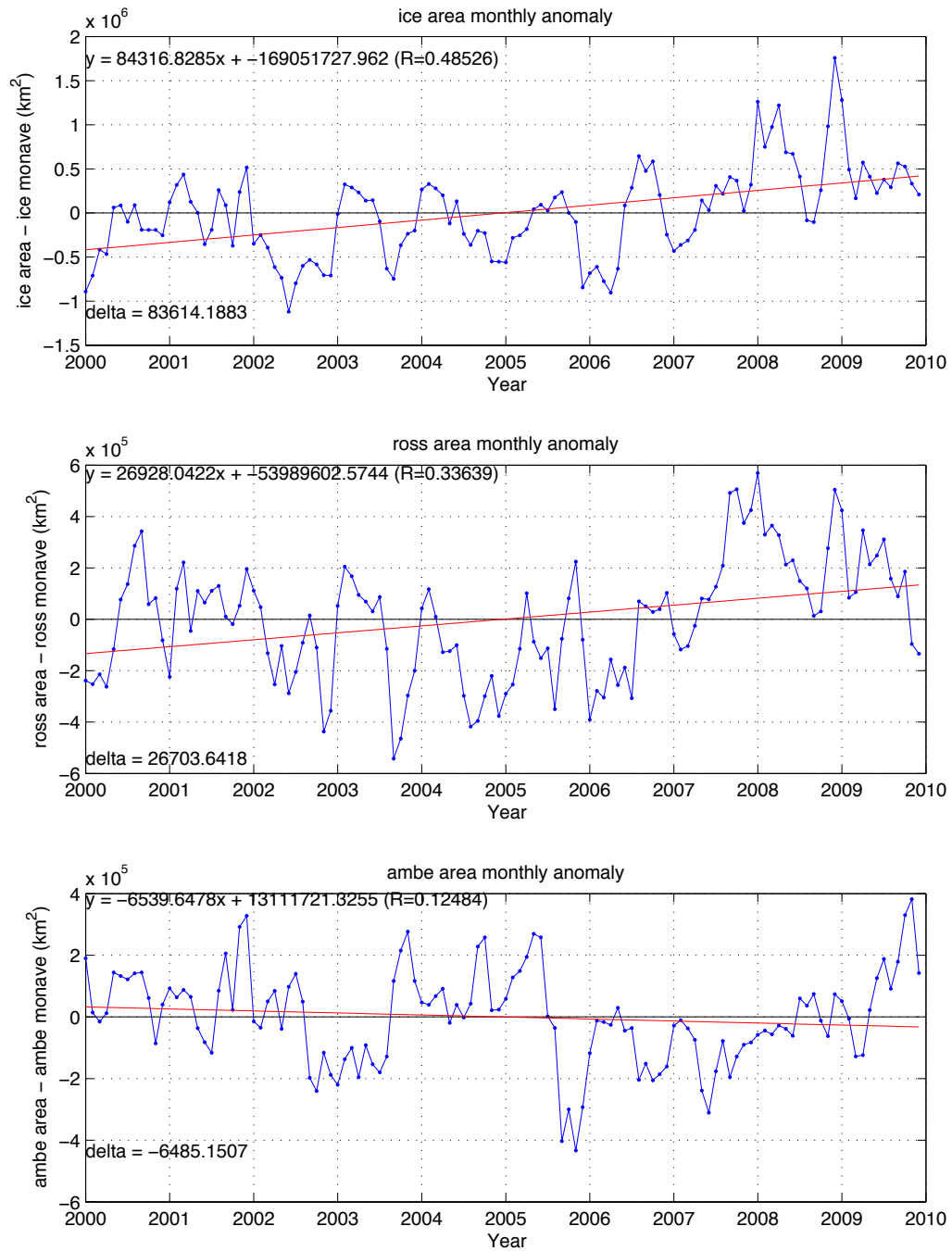


Figure 20. Monthly sea ice area anomaly (km²) for the Southern Ocean (top), the Ross Sector (middle) and the Amundsen/Bellingshausen Sector (bottom) based on the 2000-2009 NIC concentration data. The red line is the linear fit to NIC curve.

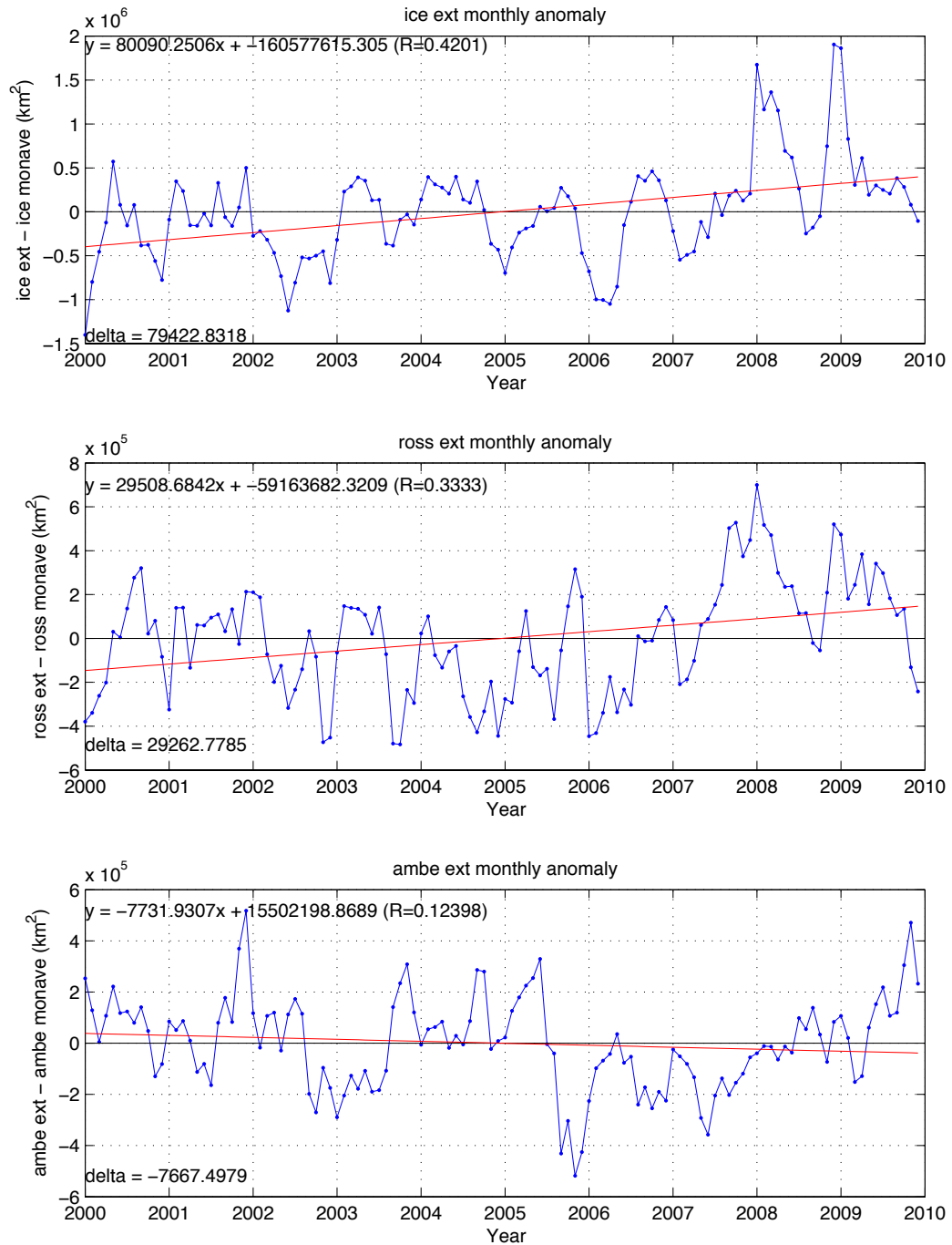


Figure 21. Monthly sea ice extent anomaly (km^2) for the Southern Ocean (top), the Ross Sector (middle) and the Amundsen/Bellingshausen Sector (bottom) based on the 2000-2009 NIC concentration data. The red line is the linear fit to NIC curve.

enough to reverse the 2000-2007 negative trends estimated for the Southern Ocean (from -0.6 to 7.7 %/decade in area, and from -0.1 to 6.3%/decade in extent) and for the Ross Sea sector (from -10.8 to 9.1 %/decade in area, and from -9.4 to 8.5 %/decade in extent). In contrast the Amundsen/Bellingshausen sector retained the 2000-2007 shrinking trend, albeit somewhat less pronounced (from -18.1 to -14.6 %/decade in area, and from -19.2 to -13.4 %/decade in extent).

Variability in sea ice area and extent at inter-annual time scales is apparent in the sea ice anomaly time series (Figures 20 and 21) calculated by subtracting the record-length mean annual cycles (Figures 16 and 17) from the monthly time series (Figures 18 and 19). These anomalies are most likely related to the dominant modes of atmospheric inter-annual variability.

The long-term (2000-2009) trends in these two sea ice anomalies (red lines in Figures 20 and 21) are positive (growth) for the Southern Ocean and the Ross sector, but negative (decay) for the Amundsen/Bellingshausen sector. These trends were calculated from linear fits to the monthly values of each sea ice property anomaly (blue dots).

4.2 Duration of Sea Ice Seasons

The length of the sea ice growth and decay seasons is calculated as the number of days between sea ice extent maxima and minima [Stammerjohn *et al.*, 2008]. The new NIC database (Figure 22, Table 7) reveals that the Southern Ocean record-length average growth season is 211 days long. The longest (shortest) growth was 231 (182) days in 2006 (2008). The record-length average decay season is only 155 days long. The longest (shortest) decay was 182 (133) days in 2008 (2006). Average season lengths are similar in the Ross Sea, but the average growth (decay) in the Amundsen/Bellingshausen is about one week (two weeks) shorter (longer). The range of seasonal maximum and minimum lengths is also greater in the Amundsen/Bellingshausen.

Table 7. Length of sea ice seasons.

	Growth Season (days)			Decay Season (days)		
	Average	Max.	Min.	Average	Max.	Min.
Southern Ocean	211	231	182	155	182	133
Ross	210	245	154	156	203	119
Amundsen/Bellingshausen	203	280	133	168	259	91

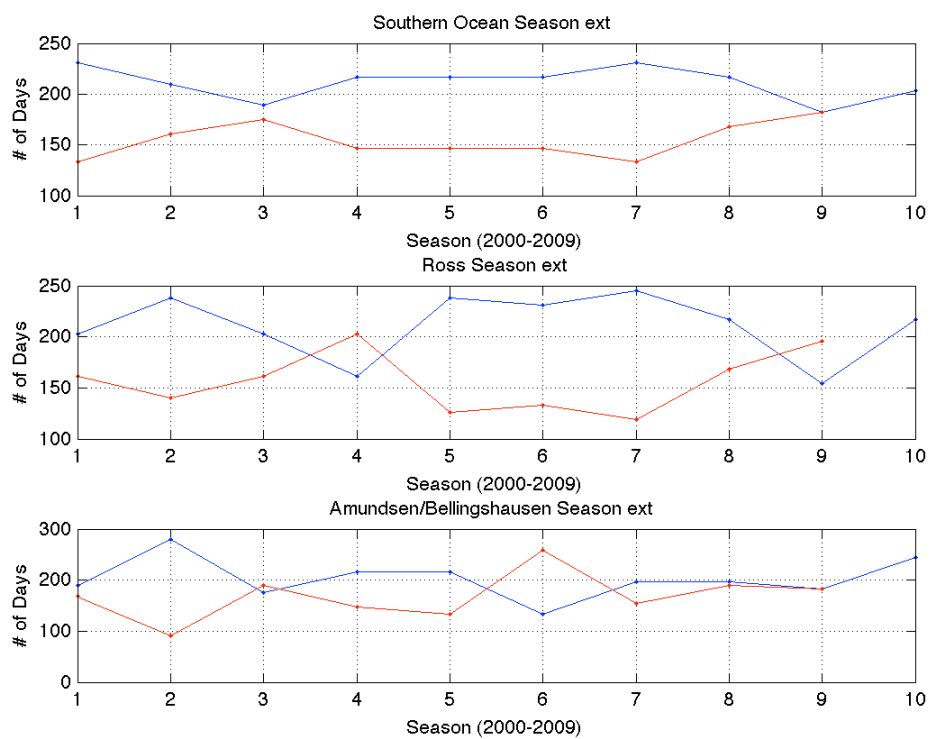
**Figure 22.** Length of sea ice growth/decay (blue/red) season determined by the number of days between maximum and minimum sea ice extent for the Southern Ocean (top), Ross Sector (middle), and Amundsen/Bellingshausen Sector (bottom).

Table 8. Surface area (10^6 km^2) of selected regions.

	Oceanic	Shelf
Southern Ocean	25.7	2.5
Ross Sea	4.4	0.5
Amundsen/Bellingshausen	2.3	0.5

4.3 Surface Coverage

The percentage of surface covered by sea ice is calculated for the entire Southern Ocean and for the two selected regions, each of which is also separated into shelf and oceanic regimes (Table 8).

The shelf regions (Figure 23) never reach 100 % of surface coverage due to the common presence of large open water leads and coastal polynyas. Sea ice covers 90 % to 94 % of the Southern Ocean shelf area for 3-5 months each year. However, over the Ross (Amundsen/Bellingshausen) shelf the winter maxima surface coverage remain at 90 % to 96 % for 7-9 months (90 % to 95% for 5-7 months) each year. Yearly differences in maximum winter surface coverage indicate possible changes in the size of polynyas over time. The Southern Ocean summer minimum surface coverage is variable (40%-60%) and occurs very briefly compared to the winter maximum.

Maxima and minima in surface coverage for the oceanic regimes show (Figure 24) less inter-annual variability than in the shelf regimes. Also, the range of surface coverage variability in the Ross Sea oceanic regime is slightly larger (10 % to 80 %) than in the Amundsen/Bellingshausen (0 % to 60%) sector.

4.4 Sea Ice Thickness

The record-length mean annual cycle of area-weighted sea ice thickness in the Southern Ocean (Figure 25) shows a maximum in December, decreasing for five months

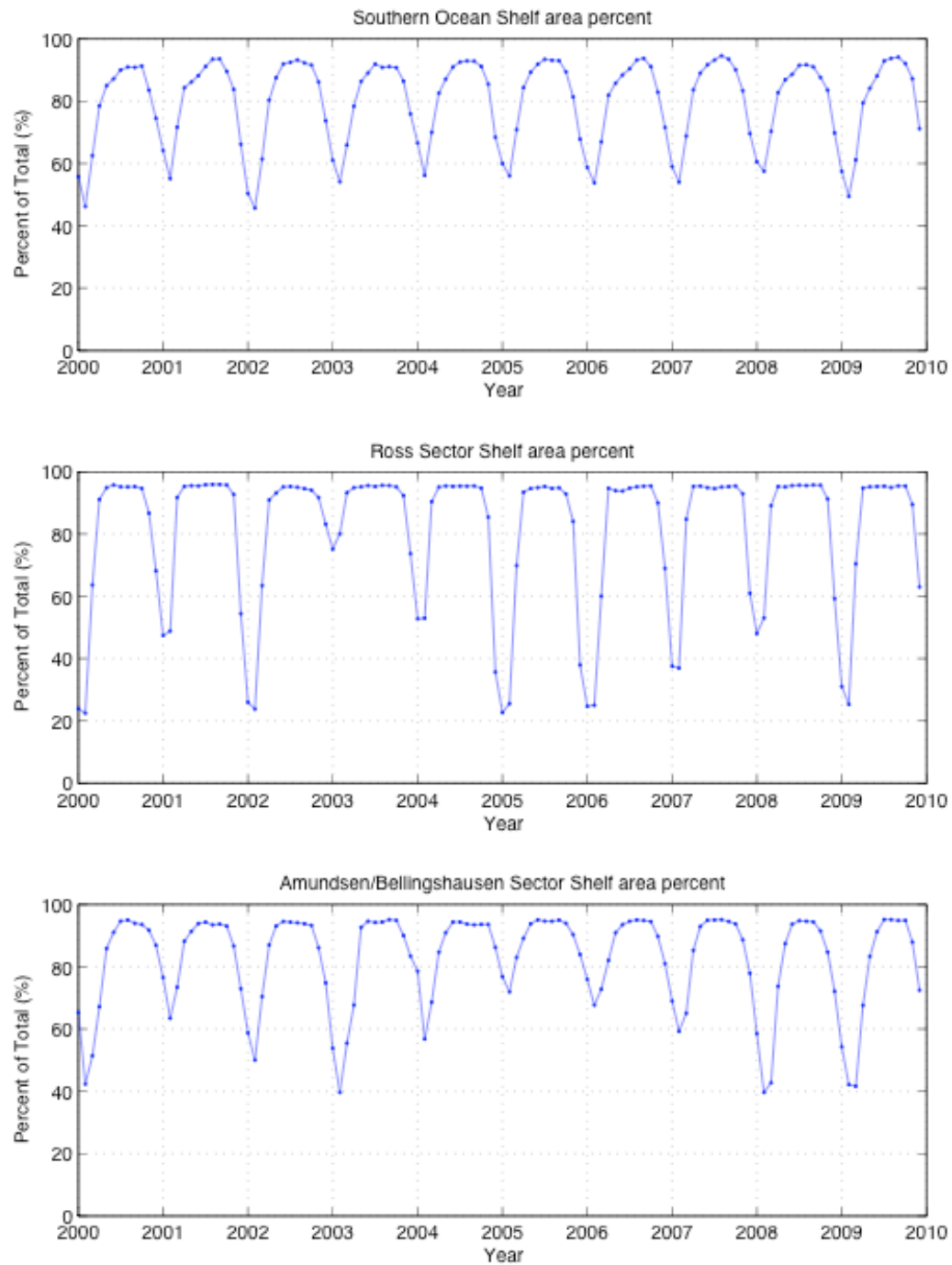


Figure 23. Monthly percent coverage (%) of total shelf area for the Southern Ocean (top), Ross Sector (middle), and Amundsen/Bellingshausen Sector (bottom).

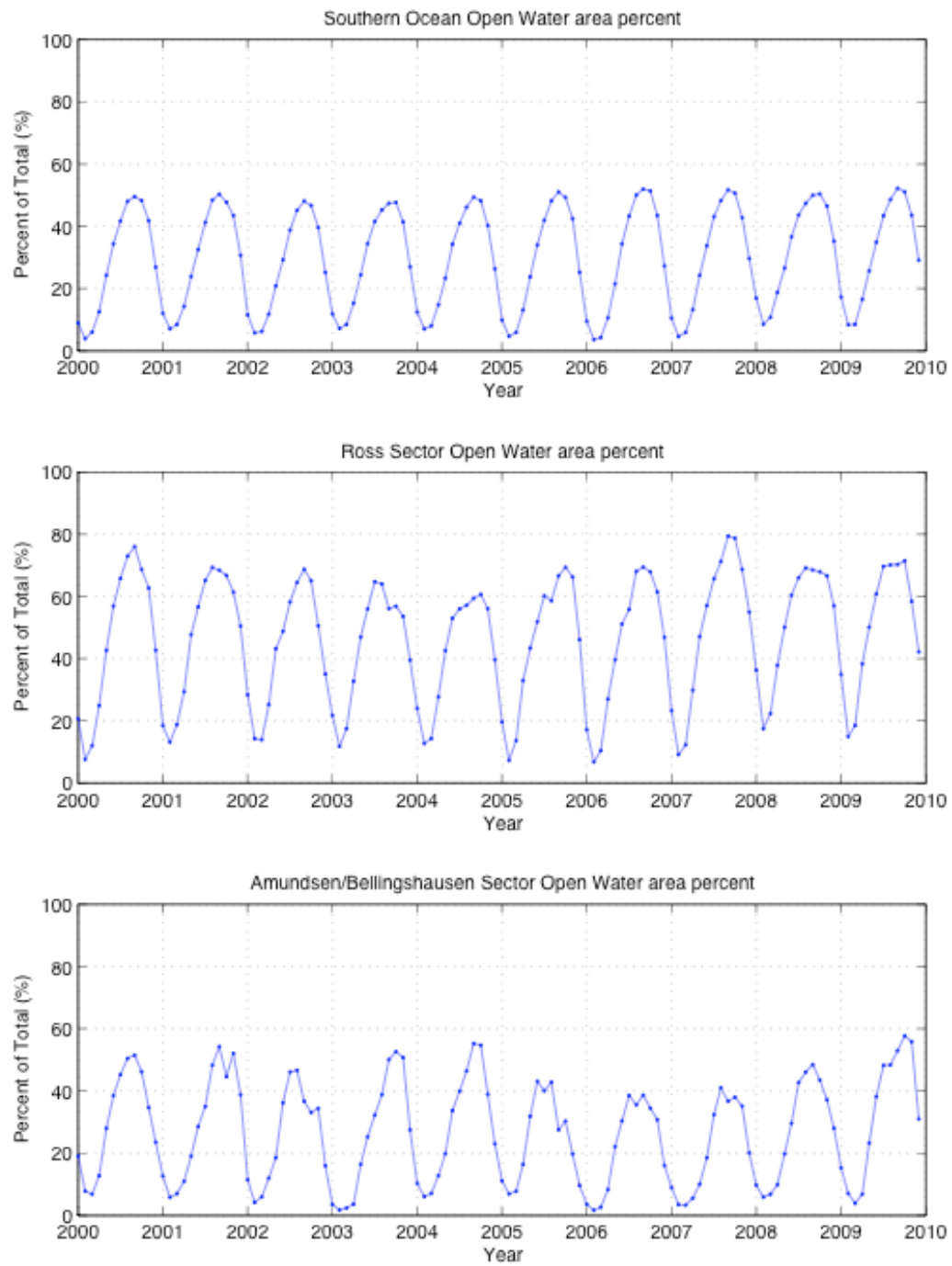


Figure 24. Monthly percent coverage (%) of total oceanic area for the Southern Ocean (top), Ross Sector (middle), and Amundsen/Bellinghousen Sector (bottom).

Table 9. Monthly NIC sea ice thickness statistics.

THICKNESS	Mean	Maximum		Minimum	
	cm	month-year	cm	month-year	cm
Southern Ocean	66.7	Nov-04	97.9	Apr-02	40.2
Ross	71.3	Oct-04	109.8	Mar-02	32.1
Amundsen/Bellingshausen	65.1	Nov-04	100.1	Mar-02	36.1

to a minimum in May, followed by seven-month of increase. Thus the thickness annual cycle lags approximately 3 months behind those for the area and extent (Figures 16 and 17). The May thickness minimum is due to the rapidly expanding coverage of thin newly formed ice in the early winter; whereas the December thickness maximum results from rapidly shrinking areas with the thickest ice left by late spring. The maximum (minimum) thickness in the Amundsen/Bellingshausen (Ross Sea) occurs one month later (earlier) than for the Southern Ocean mean annual cycle.

The time series of monthly sea ice thickness for the Southern Ocean (Figure 26) has a record-length average of 66.7 cm (Table 9). It shows relatively high inter-annual variability throughout the record, and even more variable are the maxima and minima for the two selected regions (Table 5). Similar rising trends in sea ice thickness are determined (Table 6) for the Southern Ocean (49.2 % /decade), the Ross Sea (47.0 % /decade) and the Amundsen/Bellingshausen sectors (44.8 % /decade).

The record of monthly sea ice thickness anomalies shown in Figure 27 are calculated by subtracting the record-length mean annual cycles (Figure 25) from the monthly time series (Figure 26). Their long-term (2000-2009) trend (red lines in Figure 27) is positive (growth) for all the Southern Ocean, Ross and Amundsen/Bellingshausen sectors.

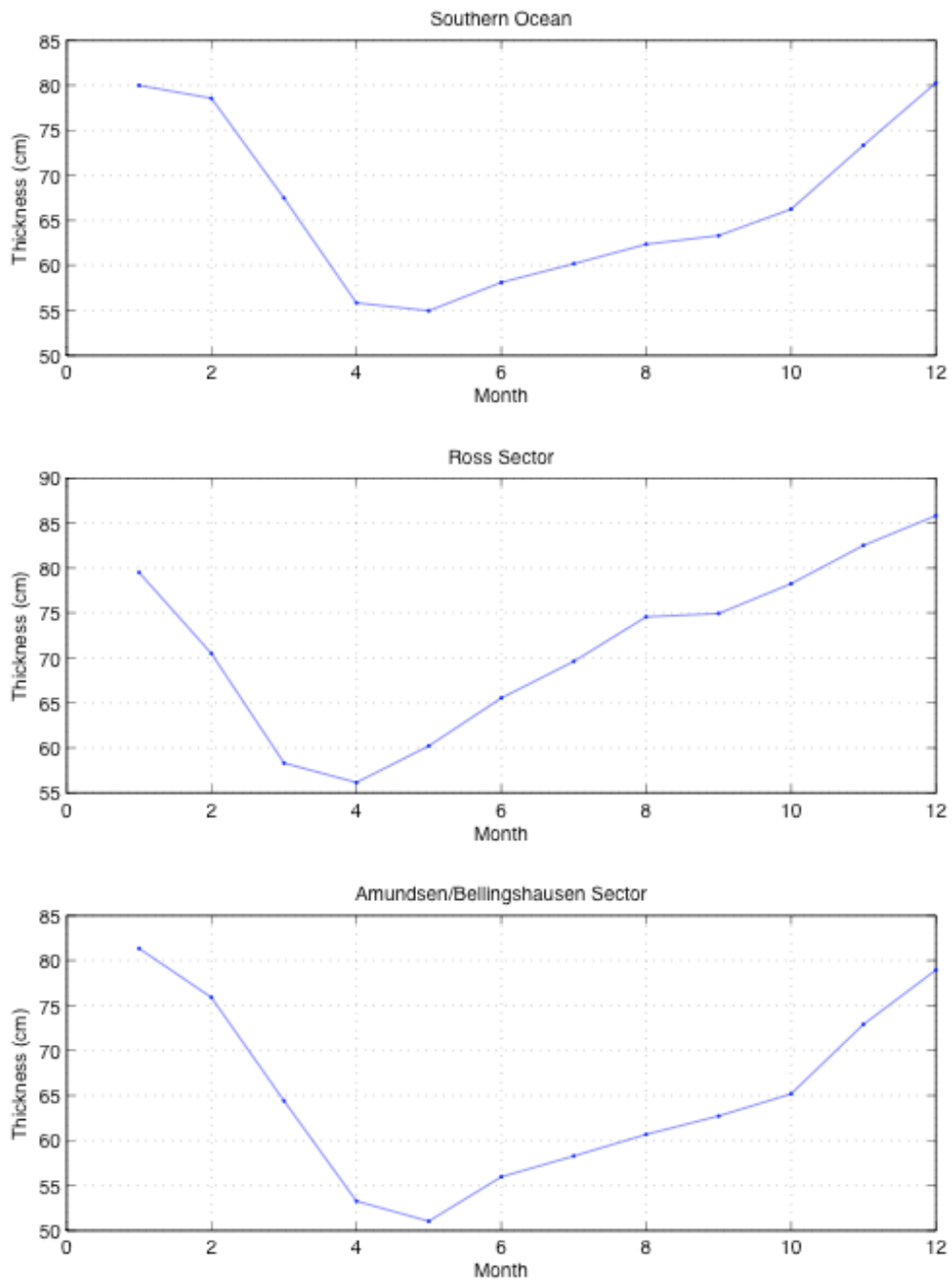


Figure 25. Record-length mean annual cycle of sea ice thickness (cm) for the Southern Ocean (top), the Ross Sector (middle), and the Amundsen/Bellingshausen Sector (bottom) based on 2000-2009 NIC data.

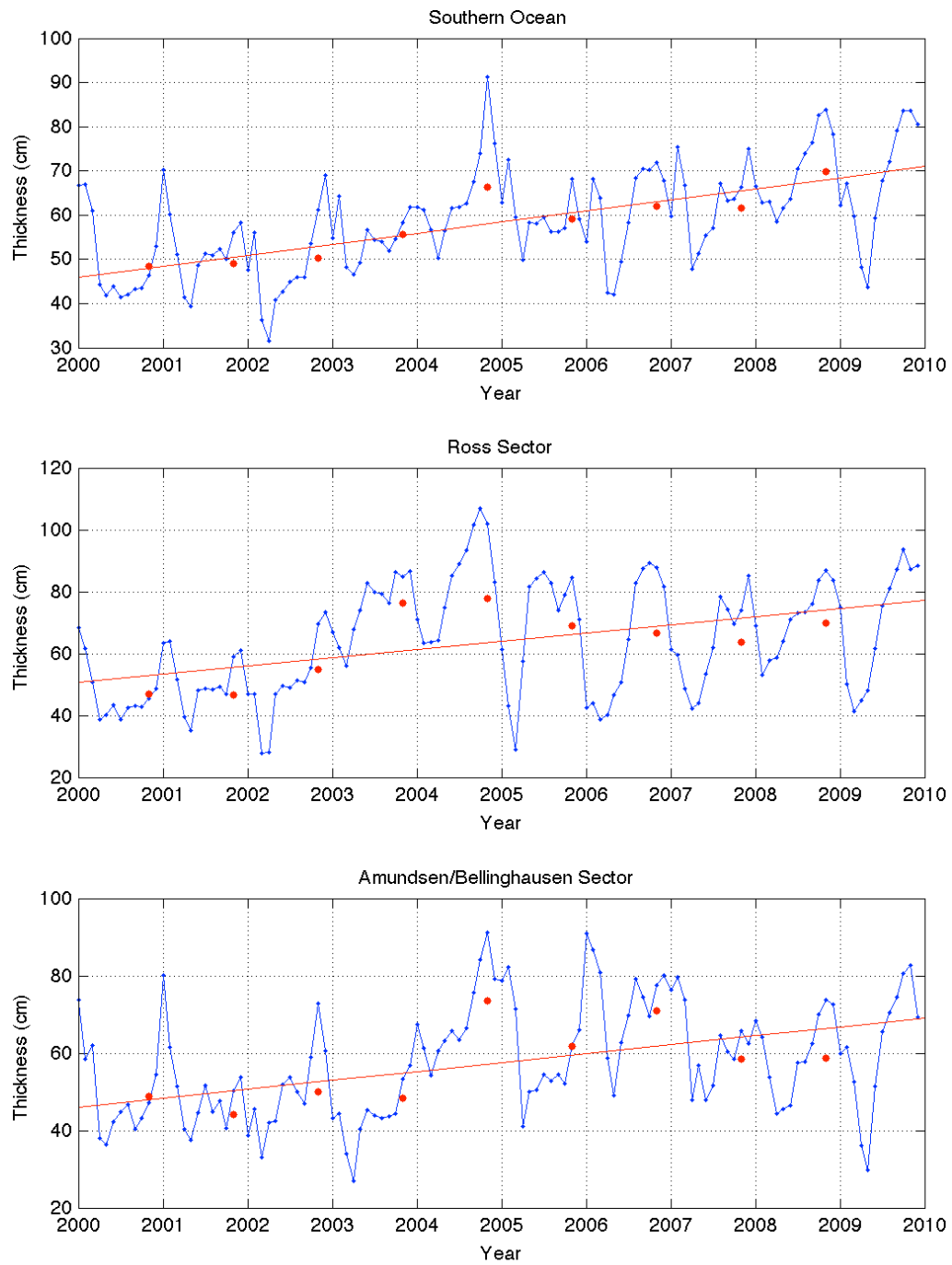


Figure 26. Monthly sea ice thickness (cm) for the Southern Ocean (top), the Ross Sector (middle), and the Amundsen/Bellinghausen Sector (bottom) based on NIC data (blue curve). The red line is the linear fit to yearly-averaged NIC data (red dots).

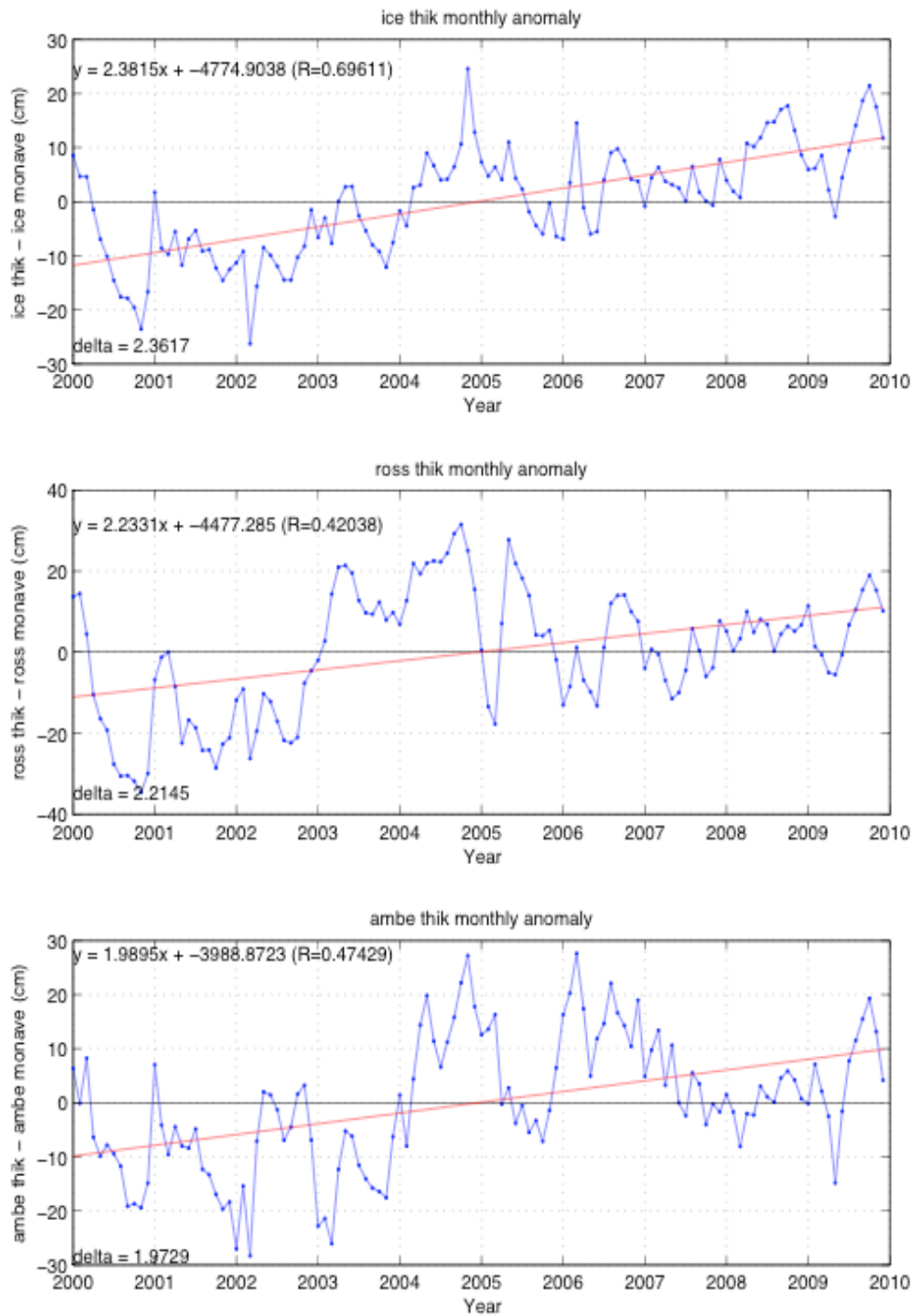


Figure 27. Monthly sea ice thickness anomaly (cm) for the Southern Ocean (top), the Ross Sector (middle), and the Amundsen/Bellingshausen Sector (bottom) based on NIC data.

4.5 Sea Ice Volume

Sea ice volume is calculated as the sum of all grid point surface area (225 km^2) times ice concentration times thickness (T_{NIC} , see Section 2.2) (Table 10). The record-length mean annual cycle for the Southern Ocean (Figure 28) sea ice volume shows a minimum (maximum) in March (November), i.e. lagging one (two) month(s) behind area and extent, and increasing (decreasing) for eight (four) months. In the Ross and Amundsen/Bellingshausen sector the average annual maximum also occurs in November, and the minimum in March.

Table 10. Monthly NIC sea ice volume statistics.

VOLUME	Mean	Maximum		Minimum	
	10^3 km^3	month-year	10^3 km^3	month-year	10^3 km^3
Southern Ocean	7.70	Oct-09	15.50	Mar-02	1.83
Ross	2.08	Oct-09	3.89	Mar-02	0.42
Amundsen/Bellingshausen	0.78	Nov-09	1.78	Mar-03	0.19

The ten-year monthly time series for volume (Figure 29, Table 6) shows that the Southern Ocean volume increased 68.3 %/decade. The two sectors also show an increase in volume: 75.8 %/decade in the Ross sector and 26.0 %/decade in the Amundsen/Bellingshausen sector. Southern Ocean sea ice volume shows a strong seasonal cycle, but also relatively high inter-annual variability throughout the record in both summer and winter peaks (Table 5). Aside from the two spikes in 2004 and 2009, which are double the record-length average, the summer maxima appear to steadily increase. Overall, the seasonal volume variability is larger than that inferred for sea ice area and extent. Both of the selected regions show higher variability in volume than the circumpolar time series, particularly during the austral winter months.

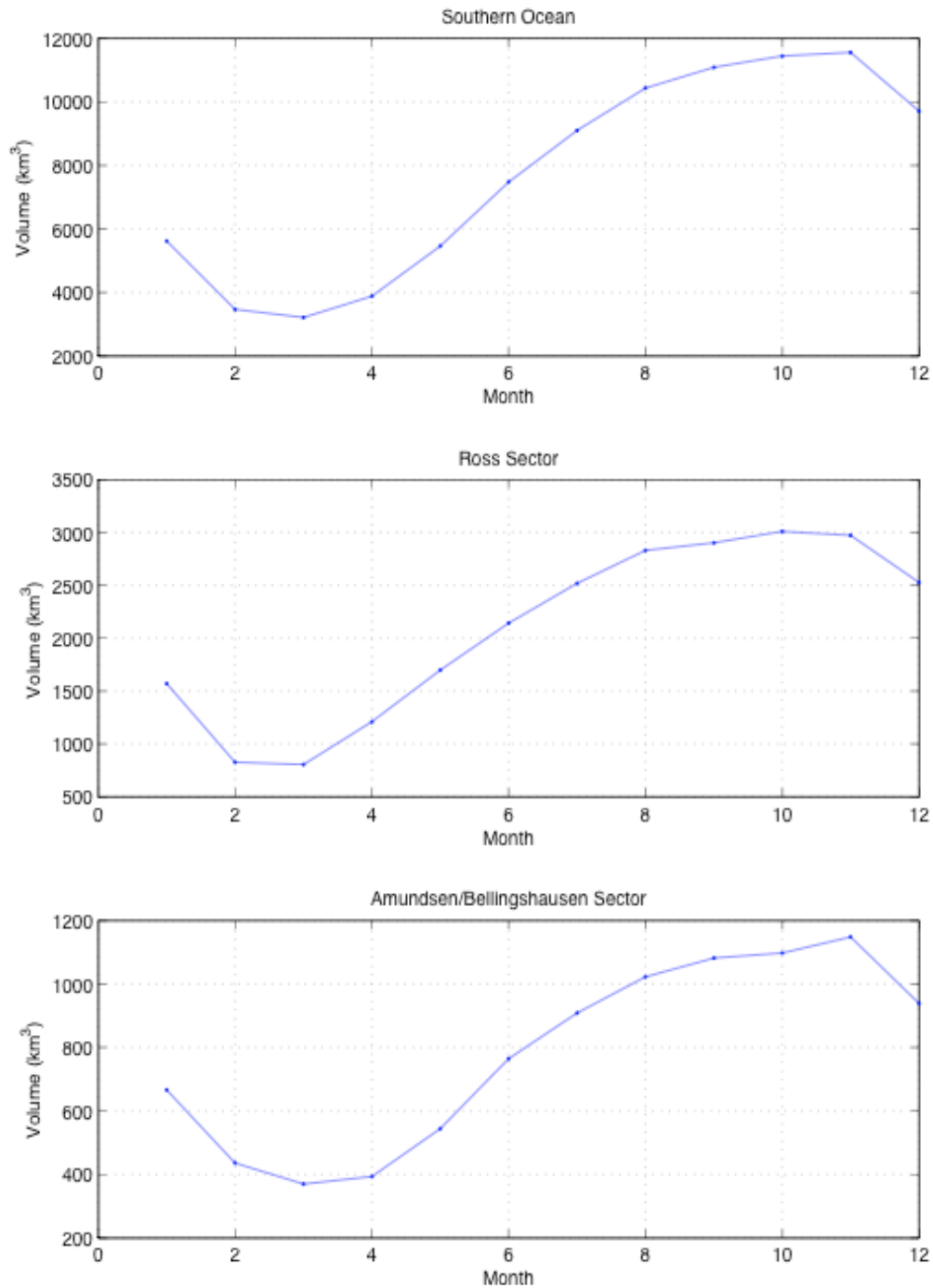


Figure 28. Record-length mean annual cycle of sea ice volume (km³) for the Southern Ocean (top), the Ross Sector (middle), and the Amundsen/Bellingshausen Sector (bottom) based on 2000-2009 NIC data.

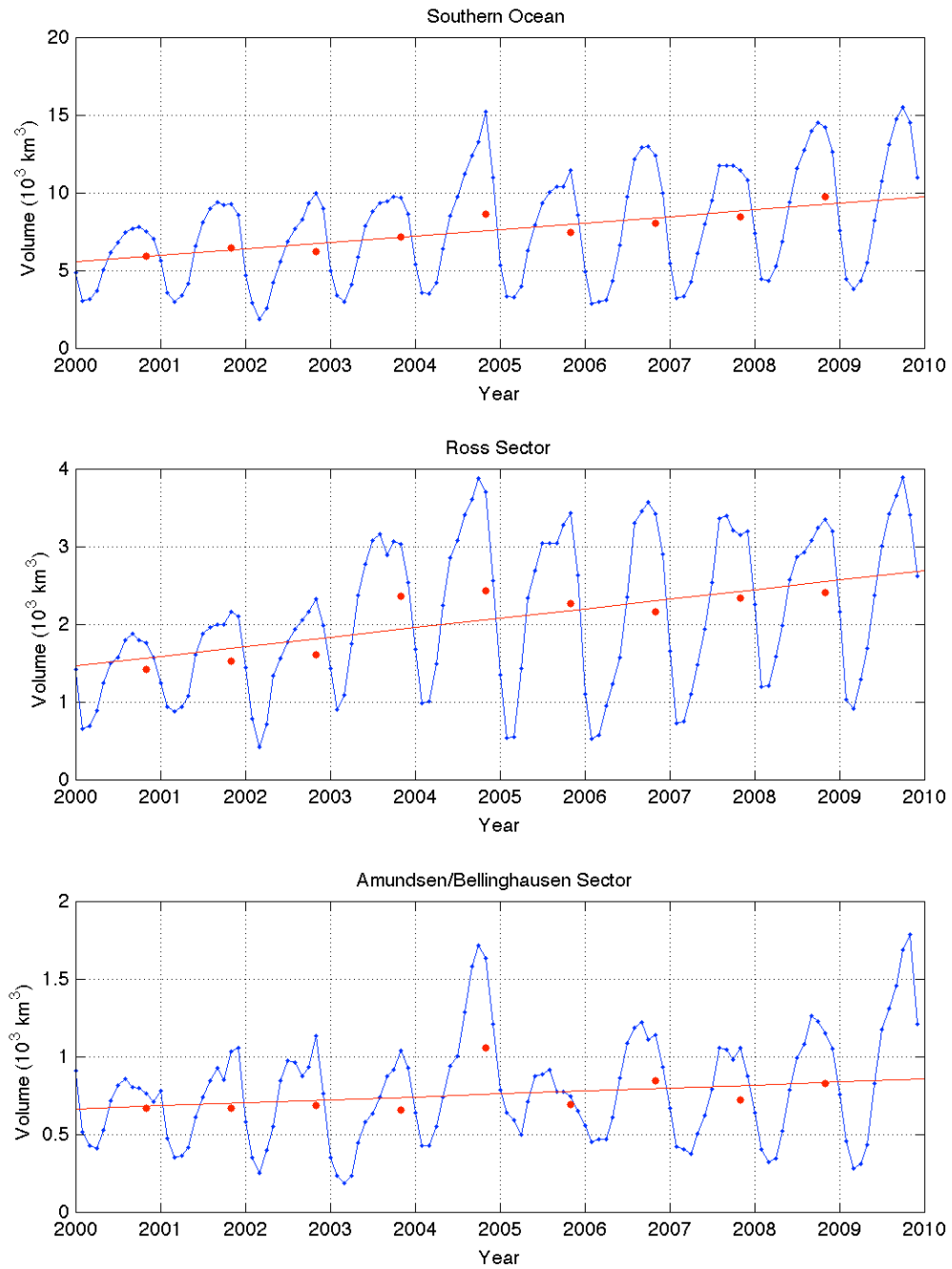


Figure 29. Monthly sea ice volume (10^3 km^3) for the Southern Ocean (top), the Ross Sector (middle), and the Amundsen/Bellinghausen Sector (bottom) based on NIC data (blue curve). The red line is the linear fit to yearly-averaged NIC data (red dots).

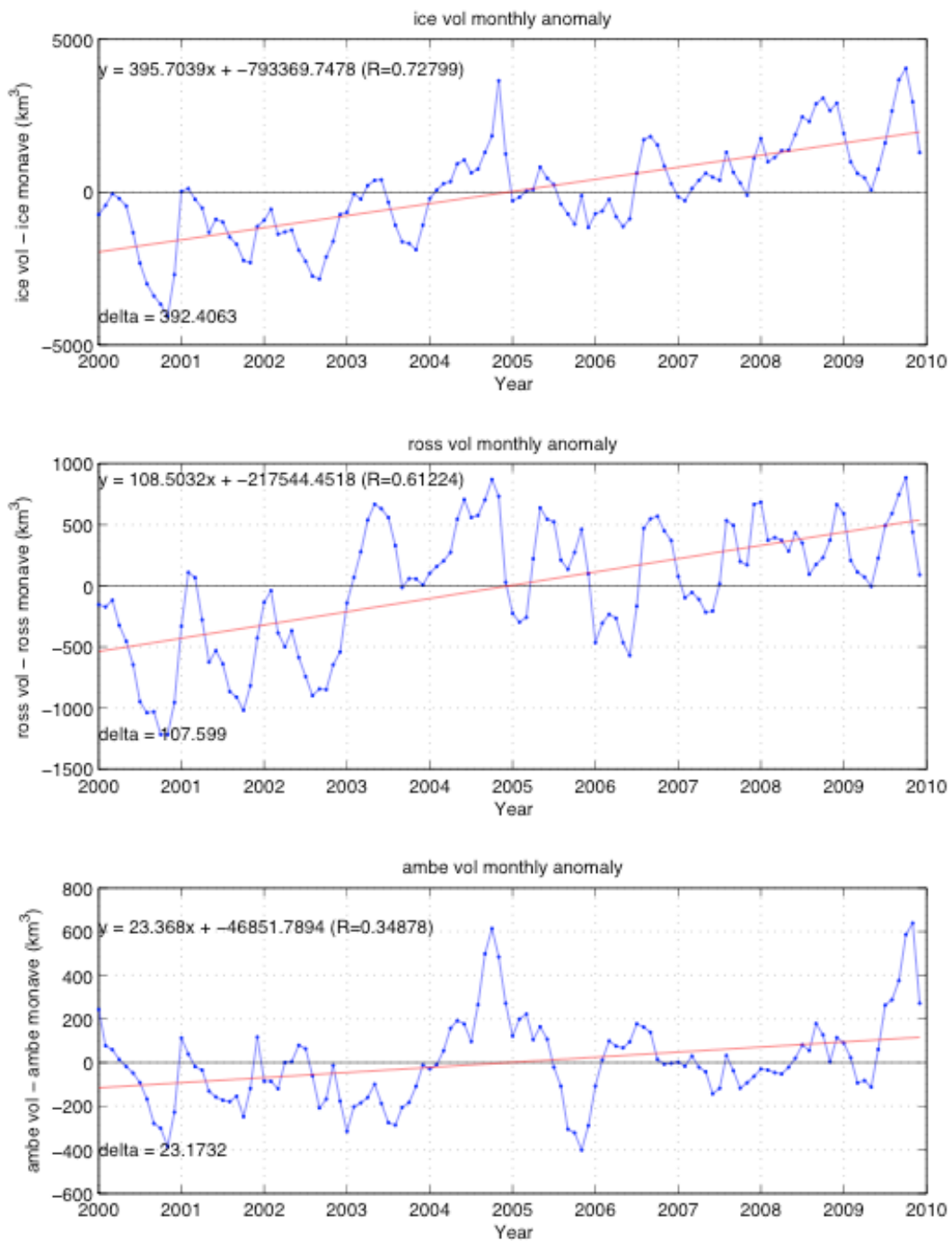


Figure 30. Monthly sea ice volume anomaly (km³) for the Southern Ocean (top), the Ross Sector (middle), and the Amundsen/Bellingshausen Sector (bottom) based on NIC data.

The monthly times series of sea ice volume anomaly (Figure 30) show similar inter-annual variability to that observed for anomaly records in sea ice extent, area and thickness.

4.6 Relationship to Atmospheric Inter-annual Variability

Previous studies of passive microwave data explore the connection between major atmospheric modes of variability and sea ice extent [*Gong and Wang, 1999; Hall and Visbeck, 2002; Kwok and Comiso, 2002; Stammerjohn et al., 2008; Yuan and Li, 2008*]. Here the fields of sea ice concentration and thickness anomalies are compared to SAM and ENSO indices (Figure 31). During the period of our time series (2000-2009) the SAM index on monthly time scales tends to favor the positive phase, whereas the ENSO index is characterized by lower frequency inter-annual variability.

The isolated impact of ENSO upon Southern Ocean sea ice is examined first. A strong negative ENSO (La Niña) year was 2000 (Figure 31). The maps of sea ice concentration and thickness anomalies for 2000 (Figure 32) shows a strong positive signal in the regions offshore the eastern Ross Sea and over the Amundsen Sea. This is consistent with the dipole associated with La Niña. However at the opposite side of the dipole, in the Bellingshausen Sea and WAP, a small negative (-7 to -16 %) concentration anomaly is observed, while concurrent sea ice thickness anomalies in that same area are mostly zero or slightly negative (-21 to +1.95 cm). Most of the circumpolar shelf regime has anomalously high ice concentration (+1 to +18 %) and thickness (+1.95 to +70.8 cm), with only a few small patches of anomalously low ice thickness (-21.0 to -44.0 cm) are found in the Bellingshausen Sea. In contrast, the largest negative thickness anomalies (-21.0 to -66.9 cm) are located over vast regions offshore of the Ross and Weddell Seas.

During 2002 the ENSO index was mostly in the positive phase (El Niño, Figure 31). A large anomalously high concentration (+1 to +26 %) region covers the Bellingshausen and WAP and the far offshore areas of the Weddell Sea (Figure 33). The Ross Sea shelf also has a large positive anomaly (+1 to +26 %), in contrast to the

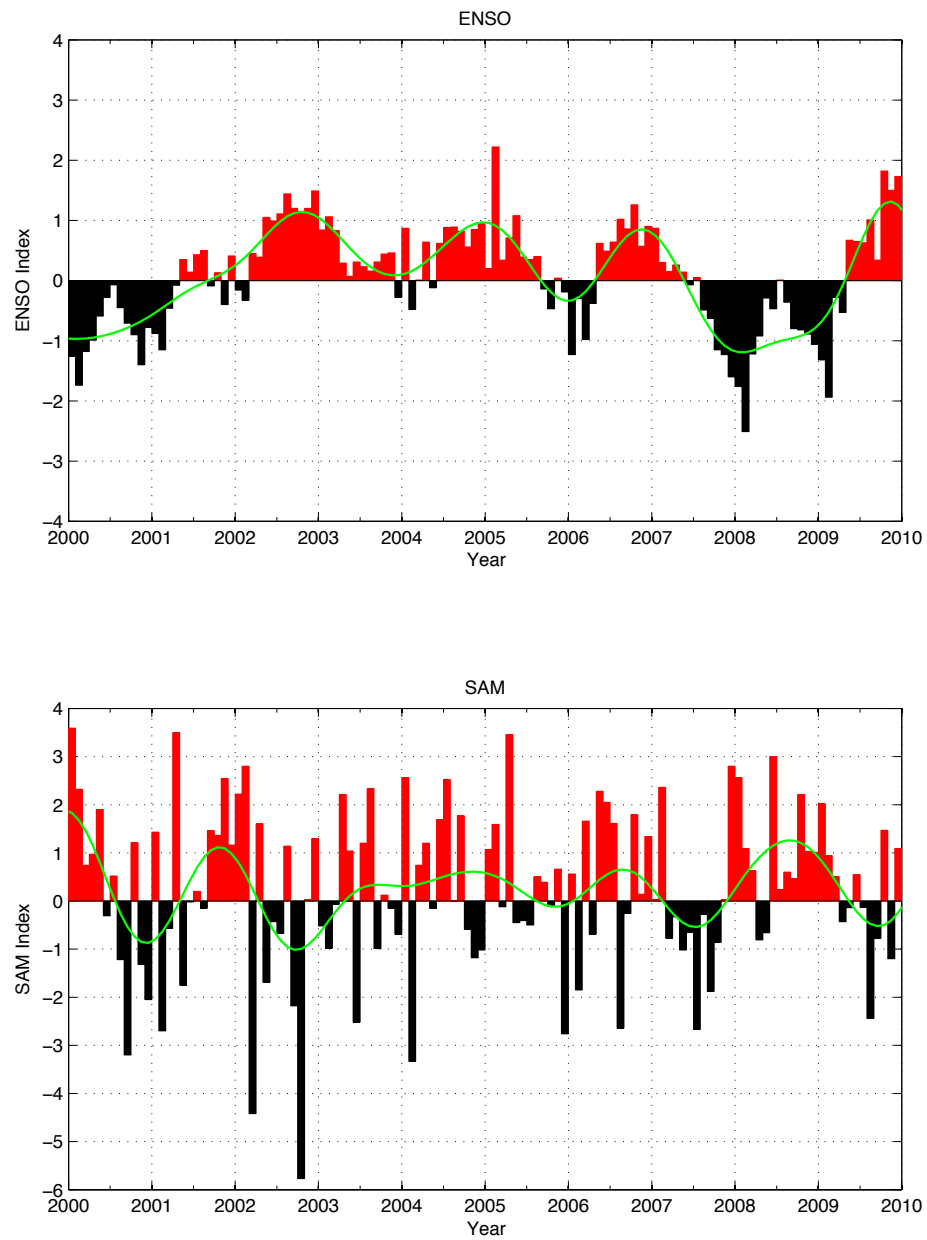


Figure 31. ENSO (top) and SAM (bottom) indices from 2000 through 2010. The green curve is the filtered data.

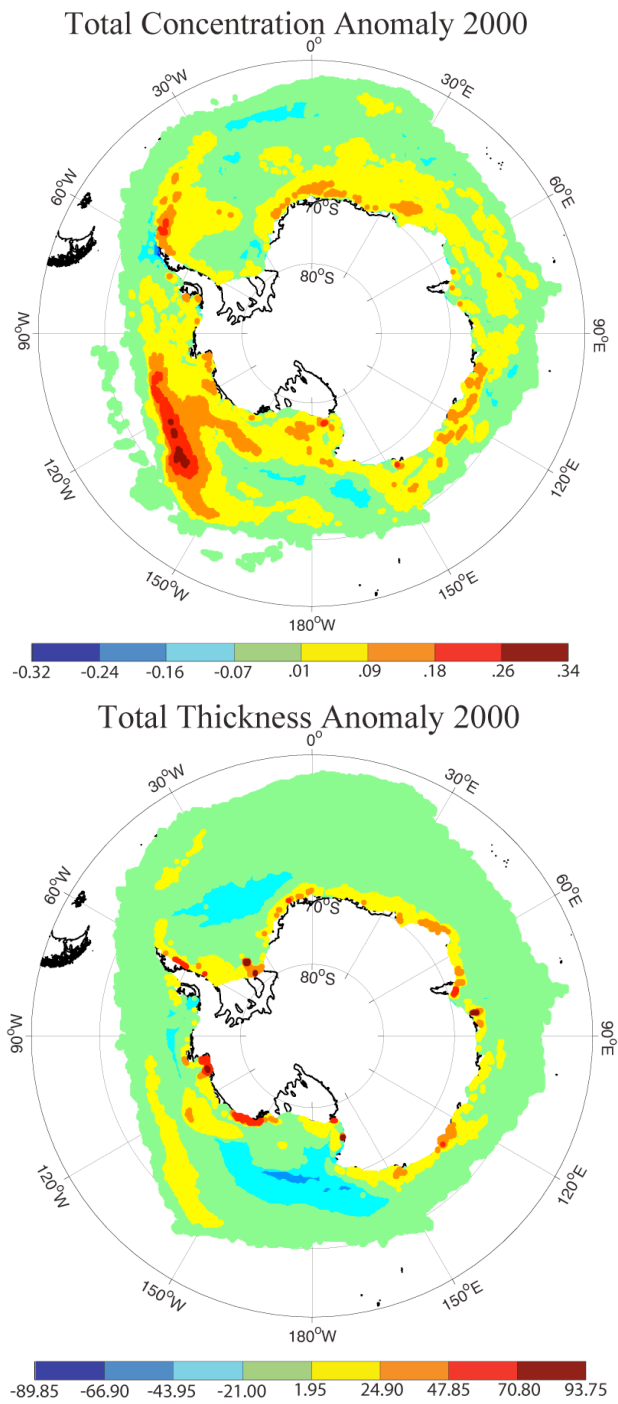


Figure 32. Total sea ice concentration anomalies (top) and thickness anomalies (bottom) in year 2000.

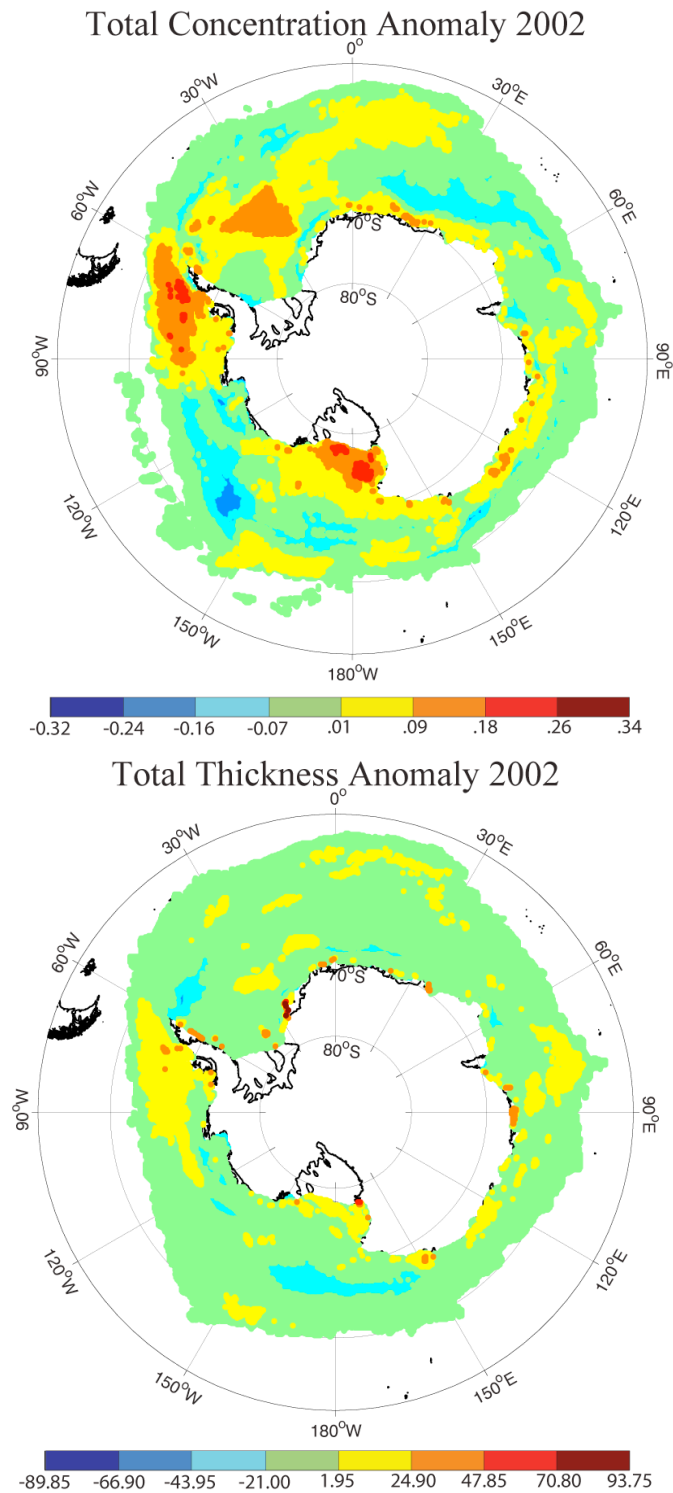


Figure 33. Total sea ice concentration anomalies (top) and thickness anomalies (bottom) in year 2002.

anomalously low concentration anomaly (-7 to -24 %) farther offshore and in the Amundsen Sea. This is also consistent with the dipole shift associated with the El Niño phase. Thickness anomalies in year 2002 are similar to those in 2000 (Figure 33), dominated mostly by near zero or slightly negative anomalies (-21.0 to +1.95 cm). A large area with positive ice thickness anomaly (+1.95 to +24.9 cm) is observed in 2002 over the Bellingshausen Sea and WAP than in 2000. In year 2002 a negative anomaly (-21.0 to -44.0 cm) relatively weaker than in 2000 shows up offshore the Ross Sea and in the Weddell just east of the tip of the Antarctic Peninsula. Also weaker in 2002 are the positive thickness anomalies over the shelf regions. Only a few small patches of thicker sea ice anomalies appeared in the offshore regions of the Atlantic, Pacific and Indian Ocean sectors.

The impact of SAM out of phase with ENSO is examined for year 2008, which like year 2000 was characterized by strong La Niña conditions. Unlike year 2000, however, the SAM index was predominantly positive in 2008 (Figure 31). Concentration anomalies in 2008 (Figure 34) are more negative in the Bellingshausen Sea and WAP than in 2000. An area of anomalously low 2008 concentrations, not seen in year 2000, is over the Ross Sea shelf region. The Weddell Sea, the Indian Ocean sector, and the offshore Amundsen/Ross Sea sectors all have anomalously high concentrations. Thickness anomalies in 2008 (Figure 34) show a more dramatic response to the out-of-phase atmospheric modes than the concentration anomalies. Two small regions of negative ice thickness anomalies (thinner ice) are centered on the Ross Shelf and the Bellingshausen Sea/WAP, overlapping with those of low ice concentration anomalies. All other shelf regions including the Weddell Sea, Indian Ocean sector and Amundsen/Ross Seas, are dominated by positive sea ice thickness anomalies (thicker ice). In the 2008 out of phase configuration, the Weddell Sea in particular shows a very strong positive response with the thickest ice anomaly.

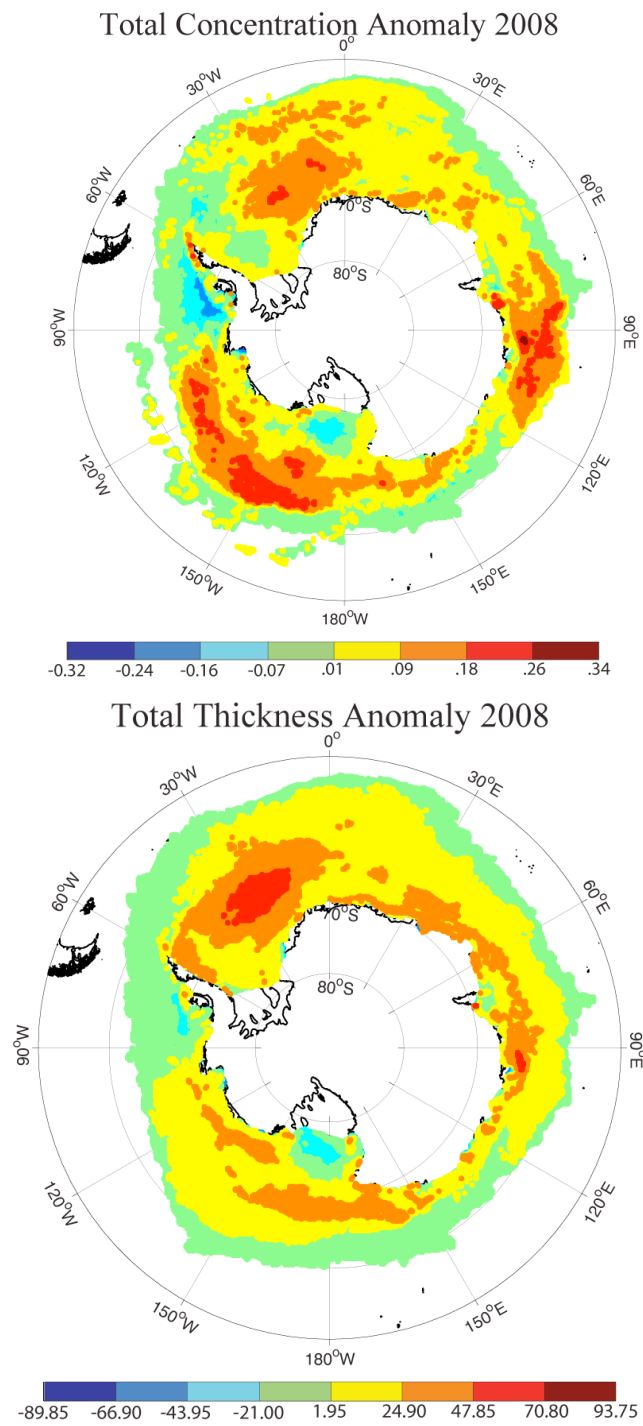


Figure 34. Total sea ice concentration anomalies (top) and thickness anomalies (bottom) in year 2008.

5. DISCUSSION AND CONCLUSIONS

Passive microwave sensors aboard a series of satellites have provided a wealth of measurements of sea ice concentration to extensively study extent and area in both polar regions. Analyses of these data emphasized the inter-connectivity of atmospheric variability and sea ice. However, technology has yet to produce an effective large-scale means of studying sea ice thickness. This study examines a prototype comprehensive ten-year time series of sea ice thickness for the Southern Ocean based on data contained within the polygons of NIC operational sea ice charts. Thickness is approximated from the three dominant stages of sea ice development and their respective concentrations.

Compared to in situ observations of sea ice thickness (ASPeCt) the new thickness proxy database shows the best agreement in the Ross Sea during the summer months, mainly because of the large number of direct observations available in that area. A linear fit correlates both datasets at 0.84 with the proxy overestimating ASPeCt data by 47.6 %. While their relationship is not robust enough to develop an ice thickness correction, the NIC sea ice concentration data is validated with NSIDC passive microwave data between 2000 and 2007. The patterns of seasonal to inter-annual variability in both monthly time series agree well with each other. Quantitatively, both data sets show similar rates of change in sea ice extent and area.

For 2000-2009 the NIC yearly mean sea ice area (extent) increased at a rate of 7.7 %/decade (6.3 %/decade) in the Southern Ocean and 9.1 %/decade (8.5 %/decade) in the Ross Sea, but it also decreased -14.6 %/decade (-13.4 %/decade) in the Amundsen/Bellingshausen. During the same period the sea ice growth (decay) season in the Southern Ocean was on average 211 (155) days long. For the Ross Sea the average length of these seasons were only one day off, but in the Amundsen/Bellingshausen Seas the growth (decay) season was on average one week shorter (two weeks longer). The surface of the Antarctic shelf regime is never fully (100%) covered during the winter due

to polynyas and open leads, but all of the selected sectors remained over 90 % covered for 3 to 9 months each winter.

Yearly average Southern Ocean sea ice thickness increased during 2000-2009 at a rate of about 2.26 cm yr^{-1} (49.2 %/decade). Thickness in the Ross Sea (Amundsen/Bellingshausen Seas) also increased at a very similar rate of 47.0 %/decade (44.8 %/decade). For the first time, a full quantification of Southern Ocean sea ice indicates an average volume of $7.70 \times 10^3 \text{ km}^3$. Moreover, sea ice volume steadily increased by $3.78 \times 10^3 \text{ km}^3/\text{decade}$ (or 68.3 %/decade). The Ross Sea (Amundsen/Bellingshausen Seas) volume also increased by 75.8%/decade (26.0%/decade).

According to this study, the response of Antarctic sea ice thickness to ENSO is relatively weak, while there is a stronger connection to SAM. In terms of inter-annual variability, a negative ENSO together with a positive SAM, as in year 2008, seems to lead to a pronounced increase in thickness and concentration. The positive trend in Antarctic sea ice thickness, and thus volume, is consistent with results from recent numerical studies investigating the effects of SAM. *Zhang* [2007] forced a global sea-ice – ocean general circulation model with 1979-2004 NCEP-NCAR atmospheric re-analyses data to simulate a 10%/decade (6%/decade) increase in Southern Ocean sea ice volume (extent). He attributed these changes to a reduced upward oceanic heat flux due to a progressively stronger stratification. A stronger hydrological cycle during positive SAM leads to increased snowfall and snow-ice formation [*Toggweiler and Russell, 2007*], a process that also increases sea ice thickness, e.g. *Powell et al. [2005]*.

Another noticeable similarity with *Zhang* [2007] is that the upward trend of sea ice volume (68.3 %/decade) estimated in this study is substantially larger than that for sea ice extent (6.3 %/decade). Although his volume increase rate is much lower (10 %/decade) than reported here, it is actually an artifact of his unrealistically large mean

volume, which clearly results from overestimating the mean annual thickness, e.g. by comparing his Figure 3 to the observation-derived product of *Worby et al.* [2008]. In fact, Zhang's simulations seem to overestimate sea ice thickness by a factor of 3, which is close to the difference in mean volume between this study ($7.7 \times 10^3 \text{ km}^3$) and his ($20 \times 10^3 \text{ km}^3$). Expressing the volume increase trends in absolute values, the $3.78 \times 10^3 \text{ km}^3/\text{decade}$ change estimated in this study is well within the $2\text{-}4 \times 10^3 \text{ km}^3/\text{decade}$ range reported in *Zhang* [2007], the latter depending on whether his numerical experiments are conducted with or without snow-ice formation. Since the rate of increase in Antarctic sea ice volume in these two independent studies are basically identical, our results support the mechanisms revealed in *Zhang* [2007].

Increased trends of sea ice volume derived in this study from NIC operational data seem to match the results of *Zhang* [2007], but caution must be exercised while interpreting the ice chart thicknesses. Besides the obvious limitations described in Sections 2 and 3, problems arise when a gradual change of ice thickness over time leads to a jump from one ice thickness category to the next. These span a wider range with increasing ice thickness (see Table 1), and can thus lead to serious biases. This problem could be diminished if the operational services used a linear ice thickness scale with e.g. 10 cm increments. On the other hand, this is not practical in view of the sparse and coarse thickness observations. This problem is presumably going to disappear once satellite-derived ice thickness data become available on a routine basis (e.g., CryoSat-2, see Section 1). For the time being, uncertainties due to snow and pressure ridges will remain. In spite of these uncertainties, any information on long-term change of sea ice thickness and volume is invaluable for determining trends and variability in the polar regions. As shown in this study, and that of *Zhang* [2007], just analyzing sea ice extent and area may yield a rather suppressed rate of change of sea ice to what might actually be occurring.

REFERENCES

- Ackley, S. F., P. Wadhams, J. C. Comiso, and A. P. Worby (2003), Decadal decrease of Antarctic sea ice extent inferred from whaling records revisited on the basis of historical and modern sea ice records, *Polar Res.*, 22(1), 19–25.
- Assman, K. M., and R. Timmermann (2005), Variability of dense water formation in the Ross Sea, *Ocean Dynamics*, 55, 68-87, doi:10.1007/S10236-004-0106-7.
- Cavalieri, D. J., C. L. Parkinson, P. Gloersen, J. C. Comiso, and H. J. Zwally (1999), Deriving long-term time series of sea ice cover from satellite passive microwave multisensor data sets, *J. Geophys. Res.*, 104, C7, 15,803-15,814.
- Cavalieri, D. J., and C. L. Parkinson (2008), Antarctic sea ice variability and trends, 1979-2006, *J. Geophys. Res.*, 113, C07004, 1-19, doi:10.1029/2007JC004564.
- Comiso, J. C., and K. Steffen (2001), Studies of Antarctic sea ice concentrations from satellite data and their applications, *J. Geophys. Res.*, 106, C12, 31,361-31,385.
- de la Mare, W. K. (1997) Abrupt mid-twentieth century decline in Antarctic sea-ice extent from whaling records, *Nature*, 389, 57–60.
- DeLiberty, T. L., C. A. Geiger, and M. D. Lemcke (2004), Quantifying sea ice in the Southern Ocean using ArcGIS, in: *Proceedings of the ESRI International User Conference*, San Diego, CA, August 9-13, 2004, 1-14.
- Dinniman, M. S., J. M. Klinck, and W. O. Smith Jr. (2007), Influence of sea ice cover and icebergs on circulation and water mass formation in the numerical circulation model of the Ross Sea, Antarctica, *J. Geophys. Res.*, 112, C11013, 1-13, doi: 10.1029/2006JC004036.
- Drinkwater, M. R., X. Liu, and S. Harms (2001), Combined satellite- and ULS-derived sea-ice flux in the Weddell Sea, *Annals of Glaciology*, 33, 125-132.
- Emery, W. J., and R. E. Thomson (2004), *Data Analysis Methods in Physical Oceanography*, Elsevier, Inc., San Diego, CA.
- Fissel, D. B., J. R. Marko, and H. Melling (2008), Advances in upward looking sonar technology for studying the processes for change in Arctic Ocean ice climate, *Journal of Operational Oceanography*, 1, 9-18.
- Gong, D., and S. Wang (1999), Definition of Antarctic oscillation index, *Geophysical Research Letters*, 26 (4), 459-462.

- Hall, A., and M. Visbeck (2002), Synchronous variability in the Southern Hemisphere, sea ice, and ocean resulting from the annular mode, *J. Clim.*, 15, 3043-3057.
- Jacobs, S. S. (2004), Bottom water production and its links with the thermohaline circulation, *Antarctic Science*, 16 (4), 427-437, doi:10.1017/S095410200400224X.
- Kwok, R., and J. C. Comiso (2002), Southern Ocean climate and sea ice anomalies associated with the Southern Oscillation, *J. Clim.*, 15, 487-501.
- Kwok, R., and D. A. Rothrock (2009), Decline in Arctic sea ice thickness from submarine and ICESat records: 1958-2008, *Geophysical Research Letters*, 36, L15501, 1-5, doi:10.1029/2009GL039035.
- Parkinson, C. L., D. J. Cavalieri, P. Cloersen, H. J. Zwally, and J. C. Comiso (1999), Arctic sea ice extents, areas, and trends, 1978-1996, *J. Geophys. Res.*, 104, C9, 20,837-20,856.
- Parkinson, C. L., and D. J. Cavalieri (2008), Arctic sea ice variability and trends, 1979-2006, *J. Geophys. Res.*, 113, C07003, 1-28, doi:10.1029/2007JC004558.
- Powell, D.C., Markus, T., and A. Stössel (2005), Effects of snow depth forcing on Southern Ocean sea ice simulations. *J. Geophys. Res.*, 110, (C6), C06001, 1-10, doi:10.1029/2003JC002212.
- Stammerjohn, S. E., D. G. Martinson, R. C. Smith, X. Yuan, and D. Rind (2008), Trends in Antarctic annual sea ice retreat and advance and their relation to El Niño-Southern Oscillation and Southern Annular Mode variability, *J. Geophys. Res.*, 113, C03S90, 1-20, doi:10.1029/2007JC004269.
- Tang, W., and D. W. Wong (2006), Exploring and visualizing sea ice chart data using Java-based GIS tools, *Computers & Geosciences*, 32, 846-858.
- Toggweiler, J. R. and B. Samuels (1995), Effect of sea ice on the salinity of Antarctic bottom waters, *Journal of Physical Oceanography*, 25, 1980-1997.
- Toggweiler, J.R. and J. Russell, (2007), Ocean circulation in a warming climate. *Nature*, 451, 286-288, doi: 10.1038/nature06590.
- Trowbridge, R. (1976), Arctic Ice Dynamics Joint Experiment (AIDJEX), *Naval Research Reviews*, 29, 8-17.
- Whitworth, T., A. H. Orsi, S.-J. Kim and W. D. Nowlin, Jr. (1998), *Ocean, Ice, and Atmosphere: Interactions at the Antarctic Continental Margin*, *Antarctic Research Series*, Volume 75, pg. 1-27, American Geophysical Union, Washington, DC.

- Worby, A. P., C. A. Geiger, M. J. Paget, M. L. Van Woert, S. F. Ackley, and T. L. DeLiberty (2008), Thickness distribution of Antarctic sea ice, *J. Geophys. Res.*, 113, C05S92, 1-14, doi:10.1029/2007JC004254.
- Yuan, X. (2004), ENSO-related impacts on Antarctic sea ice: a synthesis of phenomenon and mechanisms, *Antarctic Science*, 16 (4), 415-425, doi:10.1017/S0954102004002238.
- Yuan, X., and C. Li (2008), Climate modes in southern high latitudes and their impacts on Antarctic sea ice, *J. Geophys. Res.*, 113, C06S91, 1-13, doi:10.1029/2006JC004067.
- Zhang, J. (2007), Increasing Antarctic sea ice under warming atmospheric and oceanic conditions, *J. Climate*, 20, 2515-2529.
- Zwally, H. J., J. C. Comiso, C. L. Parkinson, D. J. Cavalieri, and P. Gloesen (2002), Variability of Antarctic sea ice 1979-1998, *J. Geophys. Res.*, 107, C5, 3041, 1-21, doi:10.1029/2000JC000733.
- Zwally, H. J., D. Yi, R. Kwok, and Y. Zhao (2008), ICESat measurements of sea ice freeboard and estimates of sea ice thickness in the Weddell Sea, *J. Geophys. Res.*, 113, C02S15, 1-17, doi:10.1029/2007JC004284.

VITA

LT Benjamin Patrick Morgan, USCG received his Bachelor of Science degree in marine and environmental science from the United States Coast Guard Academy, New London, CT in 2001. He served as a deck watch officer aboard the U.S. Coast Guard polar icebreaker *POLAR STAR* (WAGB-10) from 2001-2003, watch supervisor and operations officer at Vessel Traffic Service Houston-Galveston from 2003-2006 and as operations officer aboard the Great Lakes icebreaker *MACKINAW* (WLBB-30) from 2006-2008. He received a Master of Science degree in oceanography from Texas A&M University, College Station, TX in August 2011.

LT Morgan is currently serving in the Mobility & Ice Operations Division at U.S. Coast Guard Headquarters and may be reached at Commandant, U.S. Coast Guard (CG-5523), 2100 Second Street SW, Washington, DC, 20593. His email is benjamin.p.morgan@uscg.mil.